

Optimal Measurement-Only Topological Control of Majorana-Based Single Qubits



Peter Ferguson

Department of Physics
Lancaster University

This dissertation is submitted for the degree of
Master of Science

Acknowledgements

First I would like to thank the Lancaster University Physics department for affording me the opportunity to complete my degree here and for opening doors I previously never thought possible. In particular, I express my sincere thanks to my supervisor, Dr Alessandro Romito, without his mentorship and expertise this thesis and some of my other projects at Lancaster would not have been possible.

Thanks to Richie Dadhley for proofreading multiple drafts of this work and for the helpful discussions of the research throughout the year.

I am especially grateful for my family and friends. Without their love and support over the years, this would not have been possible. They have always been there for me and I am thankful for everything they have helped me achieve.

Abstract

Measurement-only topological quantum computation allows one to perform computations on a system of anyons—which act as a quantum computer—without physically transporting them. This is achieved using a sequence of non-demolitional topological charge measurements. This work will investigate these measurements—specifically for a system of Majorana zero modes—with the goal of optimising the inherently probabilistic process, by employing topological symmetries derived from the algebraic theory of anyon models. It is found that the probability of success is at most 50% regardless of the anyon model used. A measurement protocol that will allow one to guarantee success by simply repeating certain measurements is introduced. The only uncertainty in the system now is the number of iterations that are needed. The probability of success grows exponentially with iterations. Also, an experimental set-up is suggested that uses charge measurements on quantum dots to perform the topological charge measurements.

Table of contents

List of figures	vi
List of tables	ix
1 Introduction	1
2 Background	4
2.1 Brief Review of Kitaev Model	4
2.2 Introduction to the Algebraic Theory of Anyon Models	7
2.2.1 The Fusion/Splitting Algebra and its Operators	8
2.2.2 The Braiding Category	12
3 Model	14
3.1 Majorana Set-up	14
3.2 Braiding Operator Matrix Representation	16
4 Results	19
4.1 A Single Pairwise Projection Sequence	19
4.1.1 Anyon Models for Two-Sequences	23
4.2 Topological Symmetries of Two-Sequences	27
4.3 Topological Symmetries of Three-Sequences	29
4.4 Measurement Protocol & Experimental Realisation	33
4.4.1 Measurement Protocol	33
4.4.2 Experimental Realisation	34
5 Conclusion	38
5.1 Further Work	40
References	41

Appendix A 2-2 F-move Relation Derivation	44
Appendix B Pentagon Equation for Anyon Models	46
Appendix C Calculation of Two-Sequence Phases	47
Appendix D List of the Remaining Three-Sequences	51

List of figures

2.1	Majorana pairing for the trivial and non-trivial topological phases in the Kitaev chain (in this case the chain has four lattice sites). The black rectangles represent the lattice sites (labelled with the fermion operator for the i -th site c_i), the red dots represent the Majorana (labelled with the Majorana operators for the i -th site a_i and b_i) and the blue dotted rectangles represent the pairing between the Majorana. In (a) the chain is in the trivial topological phase and each Majorana is paired with its neighbour on the same lattice site. In (b) the chain is in non-trivial topological phase and the Majorana are paired with their neighbours on the next lattice site, leaving two unpaired Majorana on the ends of the chain.	6
(a)	Trivial Topological Phase	6
(b)	Non-Trivial Topological Phase	6
3.1	The diagram in (a) shows the set-up, a multi-terminal junction of one dimensional nanowires (red lines), which are topological superconductors hosting Majorana at the endpoints (blue dots). The centre of the junction is designed in such a way that each of the Majorana in the centre (the faded blue dots) pair up. This leaves four unpaired Majorana labelled by $\gamma_1, \dots, \gamma_4$. (b) shows how the set-up is considered on a theoretical basis. The crosses and dots represent Majorana which are ancillary and computational respectively.	15
(a)	Wire set-up	15
(b)	Majorana set-up	15

3.2	<p>The arrows represent the movement of Majorana under clockwise braiding exchange. The black dashed lines represent the superconducting phase branch cuts, that is the lines across which the superconducting phase θ—in each Majorana definition (2.3)—jumps by 2π. The crossing of the branch cut causes the γ_4 Majorana to pick up a minus sign under exchange with the γ_1 Majorana. Note that in a counter-clockwise exchange the roles of γ_1 and γ_4 are exchanged.</p>	17
4.1	<p>The diagram shows all possible results of applying the projection sequence $\Pi_{23}^{(\alpha)} \Pi_{24}^{(\mu)} \Pi_{12}^{(\nu)} \Pi_{23}^{(\beta)}$ to a general state $\psi\rangle$ in the Hilbert space of the system. The parity state $i\gamma_2\gamma_3$ is represented by α, that is the top tree shows the results for the positive parity state $\Pi_{23}^{(1)} \psi\rangle$ denoted $\alpha = 1\rangle$ and the bottom shows the negative parity state. $U_{14}^{(\pm)}$ are the clockwise and counter-clockwise braiding operators. The empty results are not braidings and so are omitted for clarity, one can find the results in (4.7).</p>	21
4.2	<p>(a) and (b) are the diagrammatic representations of the projection sequences $\Pi_{23}\Pi_{24}\Pi_{12}\Pi_{23}$ and $\Pi_{23}\Pi_{12}\Pi_{24}\Pi_{23}$ respectively. The purpose of this figure is to show that on rotating the diagrams by 180° (turning the page upside down), the above diagrams are in fact also representations of the sequences $\Pi_{23}\Pi_{34}\Pi_{13}\Pi_{23}$ and $\Pi_{23}\Pi_{12}\Pi_{24}\Pi_{23}$ when the arrows (which are omitted) are reversed, that is the anyons are replaced by their dual. This thesis is mainly concerned with the Ising anyon model (since it is the model that describes MZMs) in which every anyon is self-dual. Therefore, on rotation of the diagrams the result of the sequences is simply the inverse of the result of the non-rotated diagram. The other symmetry that should be noted here is that if one reflects the diagram in (a) in the horizontal axis from above or below the diagram and again reversing the arrows orientation the result is the same as the diagram in (b). That is, under this symmetry $\Pi_{23}\Pi_{24}\Pi_{12}\Pi_{23}$ goes to $\Pi_{23}\Pi_{12}\Pi_{24}\Pi_{23}$ and vice versa. Alternatively to see this symmetry one could place (a) “on top” of (b) and notice that they are mirror images with inversed arrow orientations. Thus if one of the sequences results in a braiding the other three do also. . . .</p> <p>(a) Projection Symmetry</p> <p>(b) Projection Symmetry for Inverted Sequence</p>	30

4.3	Exhaustive list of three projection sequences beginning with Π_{12} . Projections are represented as double arrowed numbered lines, where the numbers and colours represent the order in the sequence. The crosses and dots represent Majorana which are ancillary and computational respectively. .	31
4.4	The trajectories in these diagrams represent possible pathways from a_1 to a_4 (blue line) and from a_4 to a_1 (red line). (b) shows a two projection sequence in which is possible to find two trajectories that do not pass through the same charge line and also cross each other. If a diagram does not meet these conditions it cannot form a U_{14} braiding, for example (a) cannot form a braiding since the red and blue trajectories must pass through the purple charge line. One can find other trajectories in this sequence that do not intersect at this point but the lines must always intersect. This means one cannot form a braiding because there is no way to manipulate the two trajectories such that they resemble a braiding diagram, that is cross each other with charge lines connected them that are trivial in certain cases of measurement outcome. Note that if one uses the Π_{14} projection that the trajectories are forced to pass through a single charge line. Thus including Π_{14} in a sequence destroys the chance of braiding (a fact that was used in Sec.4.2).	32
	(a) Anyon Trajectories Example in a Three-Projection Sequence	32
	(b) Anyon Trajectories Example in a Two-Projection Sequence	32
4.5	The diagram shows the probability of achieving the desired braiding (clockwise or counter-clockwise) for the sequence of projections, say $\Pi_{23}\Pi_{12}\Pi_{24}\Pi_{23}$, as a function of the number of iterations of the protocol n . That is, the number of times $\Pi_{12}\Pi_{24}$ are repeated until the desired outcome is achieved. The probability function is a geometric series and so grows exponentially with $P(n) \rightarrow 1$ as $n \rightarrow \infty$	34
4.6	The multi-terminal junction of one dimensional nanowires (red lines) hosting MZMs at the ends (blue dots), designed in such a way that each of the MZMs in the center (the faded blue dots) pair up. Leaving four unpaired MZMs labelled by $\gamma_1, \dots, \gamma_4$. The measurement apparatus is split into two sections denoted L & R . The black circles represent quantum dots (labelled by P_a and Q_b where $a, b \in \{L, R\}$) which are weakly coupled to the MZMs by tunnelling-couplings (black dashed lines) of strength $\omega_{\alpha,\beta}$ (where $\alpha \in \{1, 2, 3, 4\}$ and $\beta \in \{Q_L, Q_R, P_L, P_R\}$).	35

List of tables

4.1 Ising Anyon Model: where $a \in \mathcal{C}$ and $e, f \in \{I, \psi\}$. The first row contains the set of particles and the values of the quantum dimension. The second row is the fusion rules of each of the particles. Then the final two rows give the phases picked up under R-moves and F-moves. All the non-trivial F-moves and R-moves are listed. Any other F-move or R-move allowed by the fusion rules above are unity and vanish otherwise. The final F-move is a matrix, this is not used in this thesis but more information can be found in [26]. 26

Chapter 1

Introduction

The differences in the nature of quantum information and classical information due to effects like entanglement, allow quantum computers to outperform classical computers in terms of calculation speed (for a comprehensive introduction to quantum computing and quantum information see [M. Nielsen \[1\]](#)). Many people contributed to the founding of quantum computation, some of the most notable are [Feynman \[2\]](#) and [Shor \[3\]](#). All computers are built on the same basic principles for computation [\[4\]](#), they are: (i) The computer consists of cells (usually bits or qubits); (ii) One can operate on several cells simultaneously; and (iii) All cells are identical so that the same computational model is applied to all of them. The models consist of operations called gates that act on the cells. The difference between classical and quantum computing is how these principles are interpreted. Using the von Neumann axioms of quantum mechanics [\[5\]](#) the quantum interpretation is as follows: (i) The cells are described by a small dimensional Hilbert space (two-dimensional in the case of qubits) and the entire computer is described by the tensor product of each of the cells' Hilbert spaces; (ii) Each operation is described by a unitary operator on the Hilbert space of the selected cell tensored with the identity in every cell that is not acted on; and (iii) A p -qubit gate is defined as some unitary operator acting on the Hilbert space of a set of p qubits. In [Chap.3](#) these principles are used when considering the minimal complexity set-up considered in this thesis. These principles constitute an idealistic view in terms of complexity theory but they are not always physically possible, due to effects such as decoherence and noise in the system. These effects cause a loss of quantum behaviour of the system through interactions with the environment, which cause the relative phase between different states to change.

One goal of modern quantum computing research is to find a way to negate the effects of noise and decoherence, called fault-tolerant quantum computation. One promising line of research is that of topological quantum computation (TQC). [Kitaev \[6\]](#) proposed

that a system of exotic particles that are neither fermions nor bosons (called anyons) could act as the quantum computer. The information could be encoded in the degenerate ground-state space spanned by the anyons, which is separated from the other states in the spectrum by an energy gap—systems with this feature are said to be in gapped phase. Hence, for weak enough perturbations, the system evolves strictly in the degenerate ground-state. A system which has some symmetries and is also in gapped phase manifests some topological properties. That is, the system cannot be continuously deformed into a non-gapped phase without breaking some of the systems symmetries, this property is called topological protection. For these reasons the qubits of TQC are generally described as topologically protected qubits. For more on topology in Condensed Matter systems see [Ferguson \[7\]](#) or [Stanescu \[8\]](#). Then by measuring some properties of the anyons, one can initialise and read the qubit. To build the desired gates, one then adiabatically moves the anyons around each other—the process known as braiding. The measurements are carried out by bringing the anyons close together so that they ‘join’ and observing the result—this process is called fusion.

The anyons considered here are called Majorana zero modes (MZMs), they are particles that are formed in multiple Condensed Matter systems [\[9, 10\]](#), for example as boundary excitations of one-dimensional nanowires. The word Majorana refers to the fact that the particles are their own anti-particles, which is the defining relation of Majorana fermions, first proposed by [Majorana \[11\]](#). It is somewhat common in the literature to refer to MZMs as Majorana fermions, however this is a misnomer since MZMs are not fermionic. They are distinct objects from the Majorana fermions considered in particle physics. The zero mode part means that the particles satisfy an energy eigenvalue equation with zero eigenvalue, it is commonly said that the particles have zero energy. This fact degenerates the ground state manifold, so that a system with two MZMs will have a doubly degenerate ground state. MZMs are interesting for multiple reasons, the first being that they are their own anti-particles and the second being that they exhibit non-Abelian exchange statistics.

Exchange statistics describe how a wavefunction changes under the permutations of identical particles, for example fermions and bosons are totally anti-symmetric and symmetric under the exchange. That is, they are representations of the permutation group S_n . Anyons are representations of a generalisation of the permutation group called the braid group B_n (more on this in [Wilczek \[12\]](#)). Anyons are said to carry fractional charge and obey fractional statistics, meaning that under permutation, anyons result in non-trivial phases or matrices. These anyons are then described as Abelian and non-Abelian respectively. In terms of TQC, Abelian anyons are not very interesting

because they can only form a very limited number of gates, whereas non-Abelian anyons can be used for a much larger number [13–15].

This thesis will mainly be concerned with measurement-only TQC (MOTQC) first developed by Bonderson et al. [16]. Which is a method of braiding anyons without physically moving them but instead using a sequence of charge measurements. Throughout this thesis a diagrammatic representation of the anyonic states and operators of MOTQC will be used alongside the usual algebraic representation.

The goal of the thesis is to try to generalise these results so that one increases the chance of achieving a braiding. The generalisation process leads to the sequence leads to a discussion of which sequences can lead to a braiding followed by adding more measurements to see how these affect the probability of braiding. Chap.2 gives a formal introduction to the basic definitions needed to follow the calculations is given in Sec.2.2. It also provides a brief review of the Kitaev model and the emergence of (MZMs), which form on the ends of a one-dimensional superconducting nanowire as boundary excitations. Chap.3 will provide an introduction to the set-up under consideration and provide an argument as to why it is the minimal possible set-up, along with a brief discussion of how one physically realises the set-up. Chap.4 begins by investigating the sequence of measurements that Bonderson et al. [16] suggested forms a braiding, in multiple different formalisms. Also presented here is a measurement protocol to guarantee a braiding is introduced and a possible experimental method of performing the measurements is also discussed.

Chapter 2

Background

2.1 Brief Review of Kitaev Model

The Kitaev model (first discussed by [Kitaev \[17\]](#), one can find many reviews of the model [\[7, 8, 18, 19\]](#)) is the simplest model of a one dimensional topological superconductor. It consists of a chain of spinless fermions which each site singly occupied. The creation and annihilation operators for the i -th site are labelled c_i^\dagger and c_i respectively. These operators satisfy the usual fermionic operator algebra, that is all anti-commutators of the operators vanish except,

$$\{c_i, c_j^\dagger\} = \delta_{i,j}. \quad (2.1)$$

The Hamiltonian for a chain with N sites is as follows,

$$\mathcal{H} = \sum_{i=1}^N \left[-tc_i^\dagger c_{i+1} - \frac{\mu}{2} c_i^\dagger c_i + \Delta c_{i+1}^\dagger c_i^\dagger \right] + \text{h.c.} \quad (2.2)$$

where it is assumed $c_{N+1} = 0$, since there is no $(N+1)^{\text{th}}$ site. The chemical potential is denoted μ and t is the nearest neighbour hopping potential. Δ is the superconducting order parameter, also known as the gap function since it determines the size of the energy gap in the excitation spectrum. The gap function is complex, so it can be decomposed into its amplitude $|\Delta|$ and phase θ , $\Delta = |\Delta|e^{i\theta}$. Breaking up the fermionic operators on each lattice site into their real a_i and imaginary b_i parts (it is also convenient to absorb the superconducting phase into these operators) gives,

$$a_i = e^{-i\theta/2} c_i + e^{i\theta/2} c_i^\dagger, \quad b_i = \frac{1}{i} \left(e^{-i\theta/2} c_i - e^{i\theta/2} c_i^\dagger \right). \quad (2.3)$$

2.1 Brief Review of Kitaev Model

These new operators are self-conjugate and are the generators of a Clifford algebra, that is,

$$\begin{aligned}\{a_i, a_j\} &= \{b_i, b_j\} = 2\delta_{i,j}, & \{a_i, b_j\} &= 0, \\ a_i^2 &= b_i^2 = 1, \\ a_i^\dagger &= a_i, & b_i^\dagger &= b_i.\end{aligned}\tag{2.4}$$

This tells us that mathematically one can represent these operators—which hereafter will be referred to as Majorana operators—as matrices that are a representation of the Clifford algebra generators, a fact that will be used extensively later in the thesis.

Rewriting the Hamiltonian (2.2) (up to a constant), in terms of the Majorana operators allows us to easily identify two different topological phases of the model,

$$\mathcal{H} = \frac{i}{2} \sum_{i=1}^N [-\mu a_i b_i + (|\Delta| + t) b_i a_{i+1} + (|\Delta| - t) a_i b_{i+1}].\tag{2.5}$$

Where $a_{N+1} = b_{N+1} = 0$ since $c_{N+1} = 0$. Let's look at two special cases, where one chooses specific values for the parameters to demonstrate the topological phases.

- First let $\mu = 0$ and $|\Delta| = t$ then,

$$\mathcal{H} = it \sum_{i=1}^N b_i a_{i+1}.\tag{2.6}$$

It is clear that since the first and last Majorana operators (a_1 and b_N) do not appear in the Hamiltonian, they are not coupled to any other Majorana and thus are called unpaired. Since they do not contribute to the Hamiltonian, one refers to them as zero modes. Hence the name Majorana zero modes (MZMs). This is a non-trivial topological phase, see in Fig.2.1(b) for a depiction of this concept.

- Second let $\mu > 0$ and $|\Delta| = t = 0$ then,

$$\mathcal{H} = \frac{-i\mu}{2} \sum_{i=1}^N a_i b_i.\tag{2.7}$$

The couplings occur on each site and neighbouring sites are uncoupled. The sites form spinless complex fermions. This called the trivial topological phase and is depicted in Fig.2.1(a)

Majorana Pairing in the Kitaev Chain

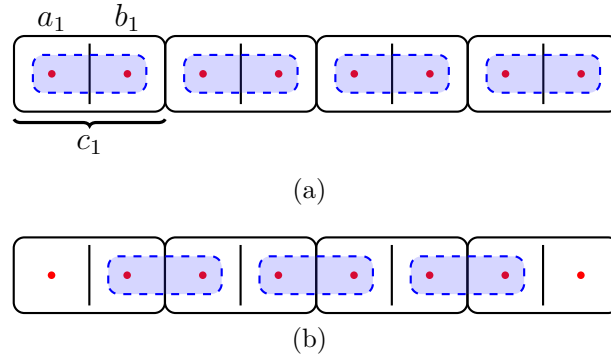


Fig. 2.1 Majorana pairing for the trivial and non-trivial topological phases in the Kitaev chain (in this case the chain has four lattice sites). The black rectangles represent the lattice sites (labelled with the fermion operator for the i -th site c_i), the red dots represent the Majorana (labelled with the Majorana operators for the i -th site a_i and b_i) and the blue dotted rectangles represent the pairing between the Majorana. In (a) the chain is in the trivial topological phase and each Majorana is paired with its neighbour on the same lattice site. In (b) the chain is in non-trivial topological phase and the Majorana are paired with their neighbours on the next lattice site, leaving two unpaired Majorana on the ends of the chain.

Since the MZMs are localised at opposite ends of the chain in gapped phase, the interaction between them vanishes exponentially with the length of the chain [17, 20]. Thus one can tune the parameters of the system so that the zero energy modes are retained as long as the gap does not close. An important note for this thesis is that one cannot form a Fock space out of an odd number of MZMs, because they form in pairs. But one can form a non-local Hilbert space using a *single* fermionic operator made out of *both* the MZMs at the end-points of the chain, $d^\dagger := a_1 + ib_N$. Of course this non-local state can either be filled or empty, but it remains at zero energy, therefore the ground state has a two-fold degeneracy. The degenerate ground states can be labelled using their fermion parity, that is the two states are labelled $d^\dagger d |0_-\rangle = 0$ and $d^\dagger d |0_+\rangle = |0_+\rangle$. This fact is the key to the MZMs' application to quantum information theory and quantum computing, as the doubly-degenerate ground-state of the system can be used as a qubit, which stores information (whether the state is filled or empty) in a way that is topologically protected by the gap against local noise and decoherence.

2.2 Introduction to the Algebraic Theory of Anyon Models

This section attempts to introduce the basics of the algebraic theory of anyon models in a concise form. The algebra is rather abstract and mainly diagrammatic. As will become clear the algebra is similar in aesthetic to the theory of Feynman diagrams; however, there are only a small number of commonalities and a much larger number of nuances between the two. The mathematical framework of the theory is well-developed and fascinating—to the author at least—but to delve into it would be a large and unnecessary detour. For those more mathematically inclined and interested in the rigorous details, the objects that are referred to here as anyon models are known formally as *unitary modular braided tensor categories*. One can find very detailed expositions on the topic by Wang [21] and Fuchs et al. [22]. Although this framework is very powerful in application, its full force is not required for this thesis. Consequently, this section will attempt to present the abstract topic in a much more accessible form, akin to the accounts given by Bonderson and Preskill [23], Eliëns [24], Ayeni [25] and Kitaev [26]. The formalism forms the algebraic core of a topological quantum field theory, which is ideal for capturing the topological properties of 2+1 dimensional many-body systems with an energy gap and short-range interactions. Thus it is perfect for studying the system of MZMs considered in this thesis.

Anyon models consist of three main components, the first specifies a finite set of particle types that are allowed. These particles are called *superselection sectors* in the mathematical parlance, but here they are referred to as *anyonic charges* or just *anyons*. The second is a set of rules governing how two of these anyons combine (fuse) to make a third, at a trivalent vertex (similar to Feynman vertices). The same rules also govern the reverse, an anyon splitting into two other anyons. The final element is a set of braiding rules that specify the exchange statistics associated with each of the anyons.

Before discussing these in more depth, let's clarify some physical points. The main focus of the model is the particle types and the topology of their worldlines¹. This means that the model ignores local degrees of freedom such as position. Also if a particle is composed of two other anyons, this is also ignored and it is considered to be its own particle type.

¹The word worldline is not particularly accurate here. The anyons are in fact considered to be fixed in space, thus the worldlines discussed here denote the movement of topological charge in time, rather than position.

2.2 Introduction to the Algebraic Theory of Anyon Models

Each of the elements of the anyon model will now be discussed in turn. First each particle worldline is graphically represented by a arrow labelled with the particle name, denoted by $i \in \{a, b, c, \dots, \mathbb{I}\} = \mathfrak{C}_A$ for example. This arrow is considered to be the worldline of the particle. Every set of particle types contains the *identity* (or *vacuum*) particle (\mathbb{I}) which is unique and denoted by the absence of an arrow (or a dashed line when necessary). Each particle i has a unique anti-particle $\bar{i} \in \mathfrak{C}_A$ represented by a arrow in the opposite direction. In these diagrams time is always assumed to travel up the page, this will be shown in the first diagram and left implicit after.



$$(2.8)$$

The final element of information in the collection of particles is the *quantum dimension* of the particles labelled d_i . Which roughly corresponds to the dimension of the particle's Hilbert space. Diagrammatically, this is written as a loop (this is proved using (2.16)),



$$(2.9)$$

2.2.1 The Fusion/Splitting Algebra and its Operators

The *fusion category* is defined on the set \mathfrak{C}_A by the *fusion rules*,

$$a \times b = \sum_{c \in \mathfrak{C}_A} N_{ab}^c c. \quad (2.10)$$

$N_c^{ab} \in \mathbb{N}$ is called the *fusion multiplicity* and denotes the number of copies of the particle c obtained in the fusion of a and b . Alternatively, one can look at it as the number of ways of combining a and b to form c . The theory is described as non-Abelian if there exists charges a and b such that,

$$\sum_{c \in \mathfrak{C}_A} N_{ab}^c > 1. \quad (2.11)$$

Henceforth the domain of the sum will be left implicit. A single charge a is said to be non-Abelian if $\sum_c N_{aa}^c > 1$. An Abelian charge a is one such that for every $b \in \mathfrak{C}_A$, $\sum_c N_{ab}^c = 1$. Now one adds some constraints to match the physical interpretation of the

2.2 Introduction to the Algebraic Theory of Anyon Models

model. The first has actually already been stated, that is, there is a unique identity particle \mathbb{I} such that, $\mathbb{I} \times a = a \times \mathbb{I}$ for all $a \in \mathfrak{C}_A$. Secondly the fusion of an anyon a and its unique conjugate charge $\bar{a} \in \mathfrak{C}_A$ gives the vacuum, $a \times \bar{a} = \mathbb{I} + \sum_{c \neq \mathbb{I}} N_{a\bar{a}}^c c$. Note there may also be other possible anyons due to the fusion multiplicity $N_{a\bar{a}}^c$. Thirdly the fusion rules must be *associative* so that the total anyonic charge is well-defined, which gives

$$d = a \times b \times c = (a \times b) \times c = a \times (b \times c) \quad \Rightarrow \quad \sum_e N_{ab}^e N_{ec}^d = \sum_f N_{af}^d N_{bc}^f. \quad (2.12)$$

Finally since one can always unambiguously define left and right in a (2+1)-dimensional system, fusion must also be *commutative*,

$$a \times b = b \times a \quad \Rightarrow \quad N_{ab}^c = N_{ba}^c. \quad (2.13)$$

There is one last equation that is required for the consistency of the model, it is called the pentagon equation. It is generally written in terms of diagrams which requires the use of F-moves which have yet to be covered here. For this reason and the fact that the equation is not required to understand the results presented in this thesis the equation is omitted (one can look to the Appendix.B or to [26] for a particularly succinct description).

The above rules define the finite-dimensional fusion Hilbert space V_{ab}^c and its dual the splitting Hilbert space V_c^{ab} , both have dimension N_{ab}^c . One can construct an orthonormal basis of the splitting space, defined by the ket $|a, b; c, \mu\rangle \in V_c^{ab}$ and similarly for the fusion space $\langle a, b; c, \mu| \in V_{ab}^c$. These are represented diagrammatically as follows,

$$\begin{array}{c} a \quad b \\ \diagdown \quad \diagup \\ \mu \\ \uparrow \\ c \end{array} = (d_a d_b / d_c)^{1/4} |a, b; c, \mu\rangle \in V_{ab}^c, \quad (2.14)$$

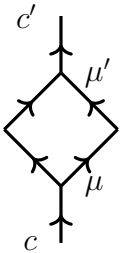
$$\begin{array}{c} c \\ \uparrow \\ \mu \\ \diagup \quad \diagdown \\ a \quad b \end{array} = (d_a d_b / d_c)^{1/4} \langle a, b; c, \mu| \in V_c^{ab}, \quad (2.15)$$

where $\mu \in \{1, 2, \dots, N_{ab}^c\}$ is the fusion multiplicity. The normalisation constant is required to maintain what is called *isotropy invariance*. This means that the diagrams are invariant under continuous deformations of the lines, so long as they do not cross the open endpoints of the diagram. To show that this is possible requires quite a bit of

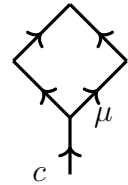
2.2 Introduction to the Algebraic Theory of Anyon Models

calculation and therefore is omitted, for details see [Bonderson and Preskill \[23\]](#). Since (2.14) and (2.15) use the language of bras and kets one can recast the model into the familiar language of quantum mechanics, which will enable us to adapt our knowledge of quantum mechanics to build a collection of rules for these diagrams. Let's begin to build some of these rules.

Since (2.14) and (2.15) define an orthonormal basis, their inner product must be a delta function. This corresponds to stacking the diagrams as follows,

$$\langle a, b; c', \mu' | a, b; c, \mu \rangle = a \text{ (diamond diagram) } b = \sqrt{\frac{d_a d_b}{d_c}} \delta_{cc'} \delta_{\mu\mu'} c. \quad (2.16)$$


This diagram leads to two immediate consequences, the first is a proof of the definition of quantum dimension, stated in (2.9). The second is the fact that there can be no ‘tadpole’ diagrams in anyon models, that is,

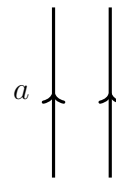
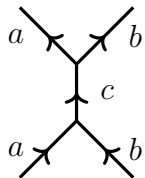
$$\langle a, b; \mathbb{I}, 1 | a, b; c, \mu \rangle = a \text{ (diamond diagram with tadpole) } b = 0. \quad (2.17)$$


This is a very important result, it means that any diagram that contains a tadpole automatically vanishes.

Now since one is working in a Hilbert space, completeness gives a resolution of the identity relation,

$$\mathbb{I}_{ab} = \sum_{c, \mu} |a, b; c, \mu\rangle \langle a, b; c, \mu| \quad (2.18)$$

Pictorially,

$$a \text{ (vertical line) } b \text{ (vertical line)} = \sum_{c, \mu} \sqrt{\frac{d_c}{d_a d_b}} \text{ (fusion diagram) } . \quad (2.19)$$



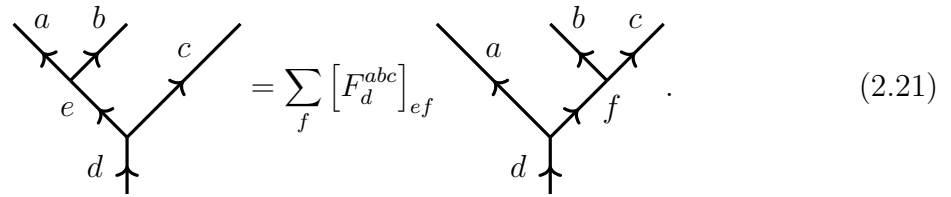
The Greek indices for the fusion multiplicities have been omitted here for succinctness (hereafter these will be omitted unless necessary). Notice that in (2.12) one considered the fusion of three anyons, but also previously stated that fusion occurs through a trivalent

2.2 Introduction to the Algebraic Theory of Anyon Models

vertex. This leads to two natural decompositions of the splitting space for an anyon d splitting into three anyons a, b, c which are isomorphic,

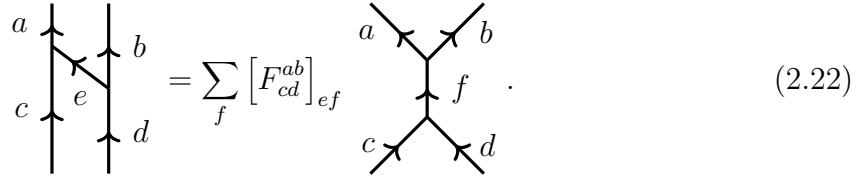
$$V_d^{abc} \cong \bigoplus_e V_e^{ab} \otimes V_d^{ec} \cong \bigoplus_f V_f^{bc} \otimes V_d^{af}. \quad (2.20)$$

Where \bigoplus_e is the direct sum of the Hilbert spaces for each particle type e . Since they are isomorphic there exists a unitary transformation between them called an *F-move* which is labelled $F_d^{abc} : \bigoplus_e V_e^{ab} \otimes V_d^{ec} \rightarrow \bigoplus_f V_d^{af} \otimes V_f^{bc}$ and defined diagrammatically as follows,



$$\text{Diagram (2.21)} \quad (2.21)$$

If the digram on the right is not permitted by the fusion rules, then the F-move vanishes. Another useful unitary is the *2-2 F-move*, it is defined as follows,



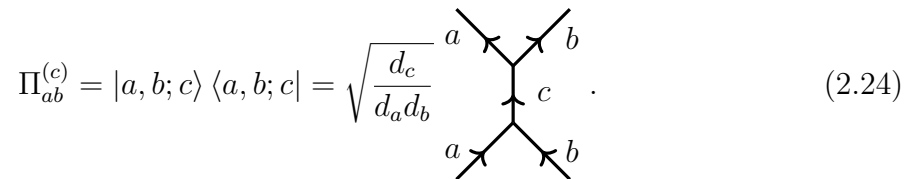
$$\text{Diagram (2.22)} \quad (2.22)$$

The 2-2 F-move is related to the F-move as,

$$[F_{cd}^{ab}]_{ef} = \sqrt{\frac{d_e d_f}{d_a d_d}} [F_f^{ceb}]_{ad}^*. \quad (2.23)$$

The derivation of this result can be found in Appendix A.

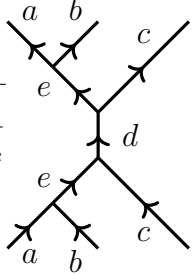
There are four more operations of interest in this thesis, they are the projection, adjoint, inverse and braiding operations. Lets first look at projections. From quantum mechanics the resolution of the identity is the sum of all projections in the Hilbert space. So(2.19), is the sum over all possible outcomes of a pairwise projection operator on the anyons a and b . Therefore a pairwise projection operator—hereafter just projection operator—is defined as,



$$\text{Diagram (2.24)} \quad (2.24)$$

2.2 Introduction to the Algebraic Theory of Anyon Models

This is described as a projection onto a and b with outcome c . One can also extend this notion to n -wise projection operators, for example a 3-wise projection operator is defined diagrammatically as,

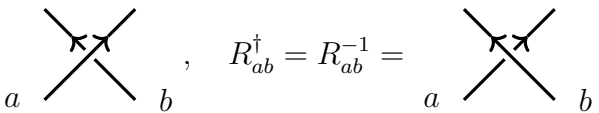
$$\Pi_{abc}^{(d)} = \sum_e \sqrt{\frac{d_d}{d_a d_b d_c}} \cdot \text{Diagram} \quad (2.25)$$


These n -wise operators are integral to a line of research discussed in Sec. 5.1.

The next operation is the adjoint. When taking the adjoint of a diagram in the theory of anyon models, one reflects in the horizontal plane—switches the top and bottom of the diagram—and reverses the orientation of all the arrows. This implies that for a diagram to be unitary, the adjoint diagram is the same as the inverse of the diagram. The inverse of a diagram, is a diagram that when combined with the original satisfies the resolution of the identity (2.19). For example, in (2.16) when c and c' are equal the bra and ket are inverses of each other.

2.2.2 The Braiding Category

The fusion category provides no relation between the fusion spaces V_c^{ab} and V_c^{ba} , this corresponds to the physical exchange of the anyons. To do this one defines the unitary braiding of a pair of anyons $R_{ab} : V_c^{ab} \rightarrow V_c^{ba}$, which is written diagrammatically as,

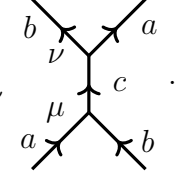
$$R_{ab} = \text{Diagram} \quad , \quad R_{ab}^\dagger = R_{ab}^{-1} = \text{Diagram} \quad (2.26)$$


These operations are referred to as *R-moves*. Thus the action of the R-move on the state $|a, b; c, \mu\rangle$,

$$R_{ab} |a, b; c, \mu\rangle = \sum_\nu [R_c^{ab}]_{\mu\nu} |b, a; c, \nu\rangle \quad (2.27)$$

2.2 Introduction to the Algebraic Theory of Anyon Models

where R_c^{ab} is the phase associated with the braiding of a and b through c . This leads to the following definition through the inner product (2.16),

$$R_{ab} = \sum_{c,\mu,\nu} \sqrt{\frac{d_c}{d_a d_b}} [R_c^{ab}]_{\mu\nu} \cdot \quad (2.28)$$


Isotropy invariance mentioned earlier allows one to continuously deform the lines without affecting the value of the diagram, as long the lines did not pass the open end points. There is a similar mechanism when the diagram contains a braiding. This is due to the fact that the R-move must satisfy the Yang-Baxter relations which are the defining relations of the braid group B_n [15], which are represented diagrammatically as, (the arrows are left implicit in these diagrams)

$$\begin{array}{c} a \quad b \quad c \\ \diagdown \quad | \quad \diagup \\ \diagup \quad | \quad \diagdown \\ a \quad b \quad c \end{array} = \begin{array}{c} a \quad b \quad c \\ \diagup \quad | \quad \diagdown \\ \diagdown \quad | \quad \diagup \\ a \quad b \quad c \end{array} . \quad (2.29)$$

This equation means that one can move lines over and under each other. In fact the same is true for vertices as seen in the following diagrams,

$$\begin{array}{c} b \quad c \quad d \\ \diagdown \quad | \quad \diagup \\ \diagup \quad | \quad \diagdown \\ a \quad b \end{array} = \begin{array}{c} b \quad c \quad d \\ \diagup \quad | \quad \diagdown \\ \diagdown \quad | \quad \diagup \\ a \quad b \end{array} , \quad \begin{array}{c} b \quad c \quad d \\ \diagdown \quad | \quad \diagup \\ \diagup \quad | \quad \diagdown \\ a \quad b \end{array} = \begin{array}{c} b \quad c \quad d \\ \diagup \quad | \quad \diagdown \\ \diagdown \quad | \quad \diagup \\ a \quad b \end{array} . \quad (2.30)$$

The collection of results that form this section act as a concise introduction to all of the theory of anyons that will be used in the following chapters, mainly in chapter 4.

Chapter 3

Model

3.1 Majorana Set-up

Similar to the set-up used by [Romito and Gefen \[27\]](#), the system used here is a multi-terminal junction made up of four, one-dimensional topological superconducting wires, in a configuration such that the endpoints of the superconductors host unpaired MZMs. The wires have a common centre, at which the MZMs on those endpoints are projected out of the degenerate ground-state space by a tunnelling Hamiltonian that pairs the MZMs together. For more details on this mechanism, one can look to [\[17\]](#), and for more on how this set-up is engineered [\[27\]](#) and the references therein. This means the set-up contains four unpaired MZMs, one for each wire, which form a four-fold degenerate ground-state manifold. Thus the system contains two qubits, a pictorial representation is given in [Fig.3.1](#). One of these qubit bits is used as an ancillary qubit and the other qubit is the one on which the braiding is to be performed, called the computational qubit.

Let us now discuss the MZMs and fermionic operators that will be used here. First note that since the MZMs are no longer paired with their neighbours on a lattice site, it makes sense to discard the previous notation in [\(2.3\)](#) that was used to distinguish the position of MZMs on the chain. The four unpaired MZMs at the ends of the wires are now represented by γ_α as seen in [Fig.3.1](#). Now, as before, one can define fermionic operators using the MZMs, let $d_{\alpha\beta} = \frac{1}{2}(\gamma_\alpha + i\gamma_\beta)$. In the Hilbert space of the two qubit system the vacuum state can be written as, $|00\rangle$ where $d_{14}|00\rangle = d_{14}|0\rangle \otimes |0\rangle = d_{23}|00\rangle = |0\rangle \otimes d_{23}|0\rangle = 0$. Thus a complete basis for the Hilbert space is given by $\{|00\rangle, d_{14}^\dagger|00\rangle = |10\rangle, d_{23}^\dagger|00\rangle = |01\rangle, d_{14}^\dagger d_{23}^\dagger|00\rangle = |11\rangle\}$. These states describe the filled and unfilled states of the fermions formed by pairing the γ_1 and γ_2 MZMs to the γ_4 and γ_3 MZMs respectively. This choice of basis was made because it is useful for the two qubits to have two different purposes, one should be computational and one ancillary.

Minimal Complexity Majorana Set-up

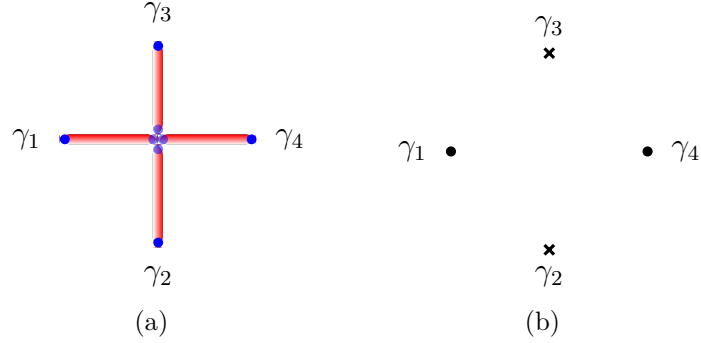


Fig. 3.1 The diagram in (a) shows the set-up, a multi-terminal junction of one dimensional nanowires (red lines), which are topological superconductors hosting Majorana at the endpoints (blue dots). The centre of the junction is designed in such a way that each of the Majorana in the centre (the faded blue dots) pair up. This leaves four unpaired Majorana labelled by $\gamma_1, \dots, \gamma_4$. (b) shows how the set-up is considered on a theoretical basis. The crosses and dots represent Majorana which are ancillary and computational respectively.

The d_{14} subspace is the computational one, that is the space in which the braiding of the MZMs is performed and then, of course, the d_{23} space is ancillary. As mentioned in Sec.2.1, the fact that the MZM operators are generators of a Clifford algebra means they can be represented as matrices—here the above basis is used to do this. Writing the MZM operators as, $\gamma_\alpha = d_{\alpha\beta}^\dagger + d_{\alpha\beta}$ and $i\gamma_\beta = d_{\alpha\beta} - d_{\alpha\beta}^\dagger$, the action of the first MZM operator on the basis states is,

$$\gamma_1 \begin{pmatrix} |00\rangle \\ |10\rangle \\ |01\rangle \\ |11\rangle \end{pmatrix} = (d_{14}^\dagger + d_{14}) \begin{pmatrix} |00\rangle \\ |10\rangle \\ |01\rangle \\ |11\rangle \end{pmatrix} = \begin{pmatrix} |10\rangle \\ |00\rangle \\ |11\rangle \\ |01\rangle \end{pmatrix}. \quad (3.1)$$

The action of the other MZM operators are derived in a similar manner, except one must note that when acting the d_{23} on the state vector $|11\rangle$, a minus sign is picked up since, $d_{23} |11\rangle = d_{23} d_{14}^\dagger d_{23}^\dagger |00\rangle = -d_{14}^\dagger d_{23} d_{23}^\dagger |00\rangle = -|10\rangle$. Then forming the matrix representation of the MZM operators using the outer product of these vectors with the

3.2 Braiding Operator Matrix Representation

basis state vector results in the following spin representation¹,

$$\gamma_1 = \begin{pmatrix} 0 & 1 & 0 & 0 \\ 1 & 0 & 0 & 0 \\ 0 & 0 & 0 & 1 \\ 0 & 0 & 1 & 0 \end{pmatrix} = \mathbb{I}_2 \otimes \sigma_x, \quad i\gamma_4 = \begin{pmatrix} 0 & 1 & 0 & 0 \\ -1 & 0 & 0 & 0 \\ 0 & 0 & 0 & 1 \\ 0 & 0 & -1 & 0 \end{pmatrix} = i\mathbb{I}_2 \otimes \sigma_y, \quad (3.2)$$

$$\gamma_2 = \begin{pmatrix} 0 & 0 & 1 & 0 \\ 0 & 0 & 0 & -1 \\ 1 & 0 & 0 & 0 \\ 0 & -1 & 0 & 0 \end{pmatrix} = \sigma_x \otimes \sigma_z, \quad i\gamma_3 = \begin{pmatrix} 0 & 0 & 1 & 0 \\ 0 & 0 & 0 & -1 \\ -1 & 0 & 0 & 0 \\ 0 & 1 & 0 & 0 \end{pmatrix} = i\sigma_y \otimes \sigma_z. \quad (3.3)$$

This thesis will mainly use the spin representation provided here rather than the Fock space states or the MZM representation. For now, let's continue to build the relationship between each. Using the matrix form of the operators γ_α and γ_β , one can define their parity $i\gamma_\alpha\gamma_\beta$, for example,

$$i\gamma_2\gamma_3 \begin{pmatrix} |00\rangle \\ |10\rangle \\ |01\rangle \\ |11\rangle \end{pmatrix} = -\sigma_z \otimes \mathbb{I}_2 \begin{pmatrix} |00\rangle \\ |10\rangle \\ |01\rangle \\ |11\rangle \end{pmatrix} = \begin{pmatrix} -|00\rangle \\ -|10\rangle \\ |01\rangle \\ |11\rangle \end{pmatrix}. \quad (3.4)$$

It is now clear that one can use this to define the following pairwise projection operator,

$$\Pi_{\alpha,\beta}^{(\pm)} = \frac{1}{2}(1 \pm i\gamma_\alpha\gamma_\beta) = \left(\Pi_{\alpha,\beta}^{(\pm)}\right)^2. \quad (3.5)$$

3.2 Braiding Operator Matrix Representation

The pairwise projections above are the main devices used in this thesis to search for a measurement-only way to braid MZMs. Let's now define what braiding means in terms of both spin representation and MZM representation following the derivation of [Ivanov \[28\]](#). Ivanov's approach calculated the braiding statistics of MZMs which form in a spinless two-dimensional $p + ip$ superconductor. However, [Alicea et al. \[29\]](#) provides a proof that the same statistics hold in one-dimensional wires when arranged in a network (the most common network is a T-junction, for more on this see [\[30–33\]](#)). First labelling the computational MZMs as in [Fig.3.1\(b\)](#), γ_1 and γ_4 . In order to braid these MZMs

¹Using the following Pauli matrix representation, $\sigma_x = \begin{pmatrix} 0 & 1 \\ 1 & 0 \end{pmatrix}$, $\sigma_y = \begin{pmatrix} 0 & -i \\ i & 0 \end{pmatrix}$ and $\sigma_z = \begin{pmatrix} 1 & 0 \\ 0 & -1 \end{pmatrix}$.

3.2 Braiding Operator Matrix Representation

one must adiabatically move them around each other, which corresponds to a unitary operation that sends $\gamma_1 \rightarrow \gamma_4$ and $\gamma_4 \rightarrow \gamma_1$. However, there is a subtlety that arises due to the presence of the superconducting phase in the definition of the MZM operators (2.3). Since shifting the superconducting phase by 2π effectively changes the sign of the operator, it is not continuous at this point and one must add a branch cut. Now, as seen in Fig.3.2, one of the MZMs must necessarily cross the branch cut of the other MZM.

Clockwise Majorana Braiding in a 2D Superconductor

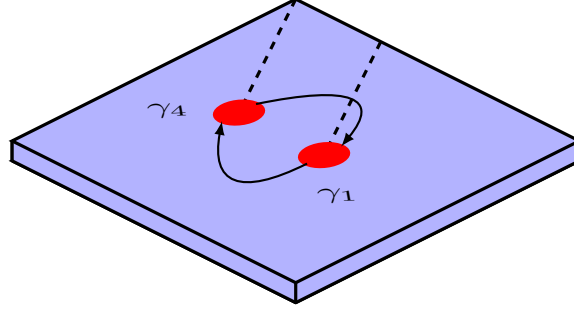


Fig. 3.2 The arrows represent the movement of Majorana under clockwise braiding exchange. The black dashed lines represent the superconducting phase branch cuts, that is the lines across which the superconducting phase θ —in each Majorana definition (2.3)—jumps by 2π . The crossing of the branch cut causes the γ_4 Majorana to pick up a minus sign under exchange with the γ_1 Majorana. Note that in a counter-clockwise exchange the roles of γ_1 and γ_4 are exchanged.

Suppose the γ_4 MZM is the one that crosses the branch cut, then the braiding transformation is the unitary which satisfies $\gamma_1 \rightarrow \gamma_4$ and $\gamma_4 \rightarrow -\gamma_1$, denoted by $U_{14}^{(+)}$, here $+$ represents a clockwise braiding (also note that for a counter-clockwise braiding—represented by $U_{14}^{(-)}$ —the opposite MZMs picks up the minus sign). To find a matrix representation of the clockwise operator, one solves the following equations,

$$U_{14}^{(+)} \gamma_1 \left(U_{14}^{(+)} \right)^\dagger = \gamma_4, \quad \text{and,} \quad U_{14}^{(+)} \gamma_4 \left(U_{14}^{(+)} \right)^\dagger = -\gamma_1. \quad (3.6)$$

To simplify the solution of these equations, assume that the unitary is block diagonal, that is $U_{14}^{(+)} = \mathbb{I}_2 \otimes U$, where $U \in SU(2)$. Then using the spin matrix representation of the MZMs the equations become,

$$U \sigma_x U^\dagger = -\sigma_y, \quad \text{and,} \quad U \sigma_y U^\dagger = \sigma_x. \quad (3.7)$$

3.2 Braiding Operator Matrix Representation

It is easy to see that these equations are satisfied when $U = \exp\left(\frac{i\pi}{4}\sigma_z\right) = \frac{1}{\sqrt{2}}(\mathbb{I}_2 + i\sigma_z)$. Recasting in terms of MZM operators the clockwise braiding operator is,

$$U_{14}^{(+)} = \exp\left(\frac{i\pi}{4}\mathbb{I}_2 \otimes \sigma_z\right) = \exp\left(\frac{\pi}{4}\gamma_4\gamma_1\right). \quad (3.8)$$

Similarly, one can see that the counter-clockwise braiding operator picks up a minus sign in the argument of the exponential so,

$$U_{14}^{(\pm)} = \exp\left(\pm\frac{i\pi}{4}\mathbb{I}_2 \otimes \sigma_z\right) = \exp\left(\pm\frac{\pi}{4}\gamma_4\gamma_1\right). \quad (3.9)$$

The purpose of this short chapter was to introduce the reader to the set-up under consideration and also the operations that are going to be performed. Next it is shown how one can use sequences of pairwise projection operators to perform a braiding on this system and calculate the probability of this occurring.

Chapter 4

Results

4.1 A Single Pairwise Projection Sequence

Let's begin with a proof of concept, that is, showing that it is possible to braid two MZMs—without physically moving them—using only a sequence of pairwise projection operators. This was first shown by [Bonderson et al. \[16\]](#) using a method that will be adopted later in order to generalise this result. First consider again the set-up in [Fig.3.1\(b\)](#), the ancillary MZMs are γ_2 and γ_3 . In terms of calculations this means that one must first project into a fixed parity state of these ancillary MZMs, then perform operations involving the computational MZMs and finally project onto the ancillary MZMs again. Since one must always include these two projections at the beginning and end of the sequence of operations a sequence of four projection is referred to as a two projection sequence (or two-sequence for short) referring to the two projections in-between the initial and final projections.

Let's consider a general state in the Hilbert space of the system which has the form $a|00\rangle + b|10\rangle + c|01\rangle + d|11\rangle$. Choosing a specific parity state of the ancilla to project into—filled, say—the general state for fixed parity becomes $|\psi\rangle = |\phi\rangle \otimes |i\gamma_2\gamma_3 = +1\rangle = c|01\rangle + d|11\rangle$. Here $|\phi\rangle$ is a general state in the computational MZMs Hilbert space. $|i\gamma_2\gamma_3 = +1\rangle$ represents the states in the ancilla Hilbert space which are filled, that is, basis states which are positive in [\(3.4\)](#). It is clear, from [\(3.9\)](#) that a braiding of this state has the following form, $U_{14}^{(\pm)}|\psi\rangle = c(1 \pm i)|01\rangle + d(1 \mp i)|11\rangle$ ¹. This thesis will follow several approaches to calculating projection sequences that lead to the braiding above. First, the fermionic operator method is used to determine whether or not a braiding takes place for the following sequence $\Pi_{23}^{(+)}\Pi_{24}^{(+)}\Pi_{12}^{(+)}\Pi_{23}^{(+)}$. Using the definitions in [\(3.5\)](#)

¹The $U(1)$ phase has been dropped. Hereafter all normalisation factors and phases will be dropped unless made explicit.

4.1 A Single Pairwise Projection Sequence

and the fermionic operators $d_{\alpha\beta}$ defined in Chap.3, it is clear that the projection $\Pi_{\alpha\beta}^{(+)}$ is just the number operator $d_{\alpha\beta}^\dagger d_{\alpha\beta}$. The action of the first operator initialises the state so one is really looking to find the action of $\Pi_{23}^{(+)}\Pi_{24}^{(+)}\Pi_{12}^{(+)} = (d_{23}^\dagger d_{23})(d_{24}^\dagger d_{24})(d_{12}^\dagger d_{12})$ on $|\psi\rangle = c|01\rangle + d|11\rangle$. First let's denote the sequence as \mathcal{P} to ease notation and note that to calculate it's action one must first find how the operators act on the basis states,

$$d_{24}^\dagger d_{24} \begin{pmatrix} |00\rangle \\ |10\rangle \\ |01\rangle \\ |11\rangle \end{pmatrix} = (\mathbb{I}_4 + \sigma_x \otimes \sigma_x) \begin{pmatrix} |00\rangle \\ |10\rangle \\ |01\rangle \\ |11\rangle \end{pmatrix} = \begin{pmatrix} |00\rangle + |11\rangle \\ |10\rangle + |01\rangle \\ |01\rangle + |10\rangle \\ |11\rangle + |00\rangle \end{pmatrix}, \quad (4.1)$$

$$d_{12}^\dagger d_{12} \begin{pmatrix} |00\rangle \\ |10\rangle \\ |01\rangle \\ |11\rangle \end{pmatrix} = (\mathbb{I}_4 + \sigma_x \otimes \sigma_y) \begin{pmatrix} |00\rangle \\ |10\rangle \\ |01\rangle \\ |11\rangle \end{pmatrix} = \begin{pmatrix} |00\rangle - i|11\rangle \\ |10\rangle + i|01\rangle \\ |01\rangle - i|10\rangle \\ |11\rangle + i|00\rangle \end{pmatrix}. \quad (4.2)$$

Thus the action of the sequence \mathcal{P} on $|\psi\rangle$ is as follows,

$$\begin{aligned} \mathcal{P}|\psi\rangle &= (d_{23}^\dagger d_{23})(d_{24}^\dagger d_{24})(c(|10\rangle + |01\rangle) + d(|00\rangle + |11\rangle)) \\ &= (d_{23}^\dagger d_{23})(c((1-i)|10\rangle + (1+i)|01\rangle) + d((1+i)|00\rangle + (1-i)|11\rangle)) \\ &= c(1+i)|01\rangle + d(1-i)|11\rangle = U_{14}^{(+)}|\psi\rangle. \end{aligned} \quad (4.3)$$

Therefore a clockwise braiding of MZMs has been achieved using only a sequence of projections—no physical movement of the MZMs. In this calculation, the outcomes of the projections were previously prescribed, which of course cannot be done when actually performing the measurement. So the next question is what is the probability of achieving a braiding when this sequence of projections is applied? To answer this one first calculates each of the eight outcomes for each initial parity state $i\gamma_2\gamma_3 = \pm 1$, then for each stage calculate the probability of each outcome. This process is rather arduous. So the results are presented as a tree in Fig.4.1 and an alternative method of calculating is developed to reduce the burden involved since this calculation will be repeated for many sequences.

The thesis will introduce two alternative methods of calculation the first being an ‘operational’ method discussed next and the second uses the anyon models introduced in Sec.2.2. The ‘operational’ method will consider the spin representation of the projection operators without applying them to a specific state. As a first example consider the generalised version of the previous sequence—generalised in that the sequence does not choose a specific outcome, $\Pi_{23}^{(\alpha)}\Pi_{24}^{(\mu)}\Pi_{12}^{(\nu)}\Pi_{23}^{(\beta)}$ where $\alpha, \beta, \mu, \nu = \pm 1$. Now Π_{23} has been

4.1 A Single Pairwise Projection Sequence

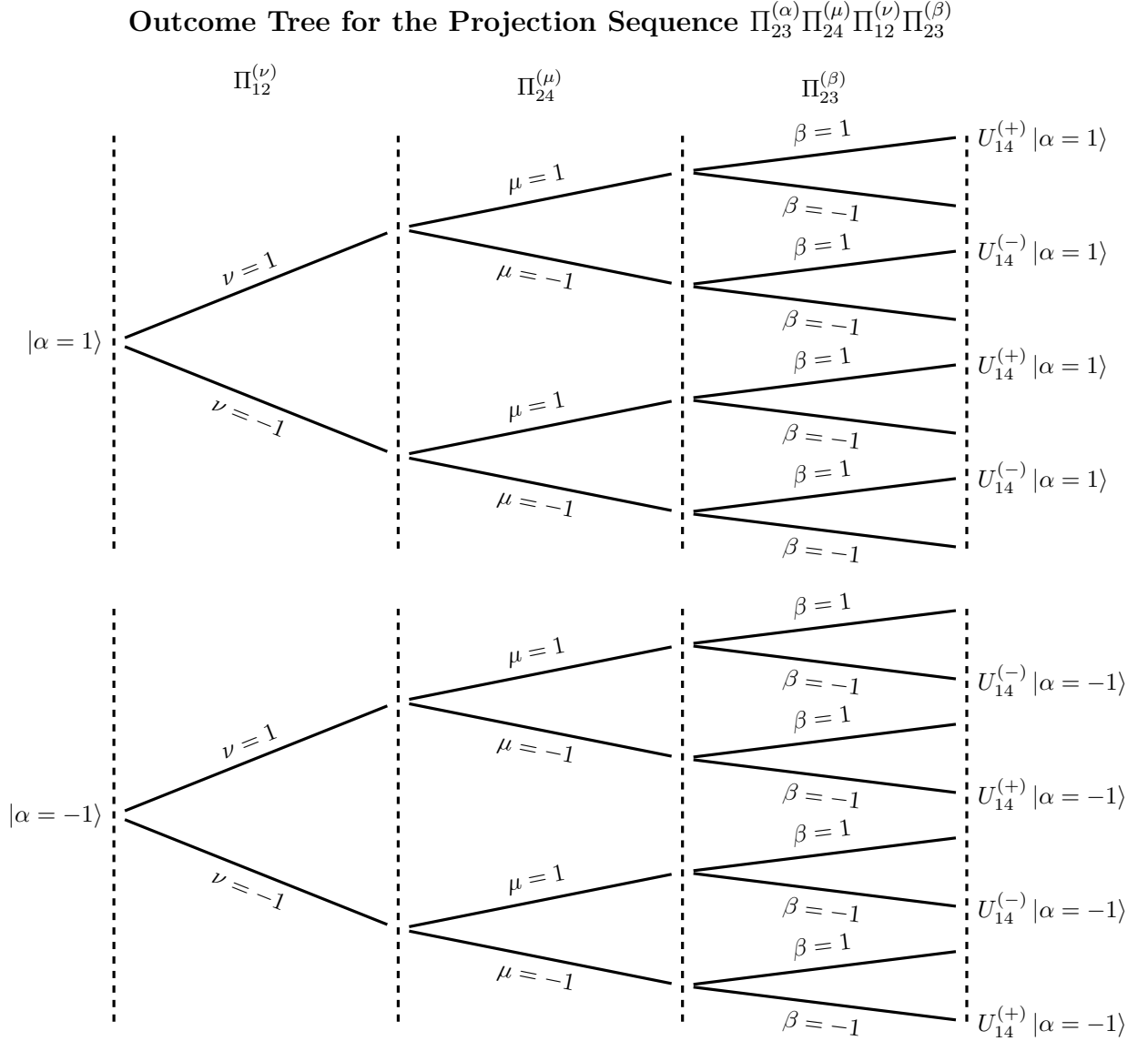


Fig. 4.1 The diagram shows all possible results of applying the projection sequence $\Pi_{23}^{(\alpha)} \Pi_{24}^{(\mu)} \Pi_{12}^{(\nu)} \Pi_{23}^{(\beta)}$ to a general state $|\psi\rangle$ in the Hilbert space of the system. The parity state $i\gamma_2\gamma_3$ is represented by α , that is the top tree shows the results for the positive parity state $\Pi_{23}^{(+)} |\psi\rangle$ denoted $|\alpha = 1\rangle$ and the bottom shows the negative parity state. $U_{14}^{(\pm)}$ are the clockwise and counter-clockwise braiding operators. The empty results are not braidings and so are omitted for clarity, one can find the results in (4.7).

chosen to be the initial and final projection and therefore will appear in every sequence so lets consider its form first,

$$\Pi_{23}^{(\alpha)} = 1 + i\alpha\gamma_2\gamma_3 = \mathbb{I}_4 - \alpha\sigma_z \otimes \mathbb{I}_2 = (\mathbb{I}_2 - \alpha\sigma_z) \otimes \mathbb{I}_2. \quad (4.4)$$

4.1 A Single Pairwise Projection Sequence

Defining the following unit matrix,

$$e_{i,j}^{(\nu)} = \begin{cases} e_i, & \nu = 1 \\ e_j, & \nu = -1 \end{cases}, \quad \text{and,} \quad e_i = \begin{pmatrix} \delta_{i,1} & \delta_{i,2} \\ \delta_{i,3} & \delta_{i,4} \end{pmatrix}, \quad (4.5)$$

allows one to represent the initial projection in the form,

$$\Pi_{23}^{(\alpha)} = e_{4,1}^{(\alpha)} \otimes \mathbb{I}_2. \quad (4.6)$$

Thus the projection sequence becomes,

$$\begin{aligned} \Pi_{23}^{(\alpha)} \Pi_{24}^{(\mu)} \Pi_{12}^{(\nu)} \Pi_{23}^{(\beta)} &= (e_{4,1}^{(\alpha)} \otimes \mathbb{I}_2)(\mathbb{I}_4 + \mu\sigma_x \otimes \sigma_x)(\mathbb{I}_4 + \nu\sigma_x \otimes \sigma_y)(e_{4,1}^{(\beta)} \otimes \mathbb{I}_2) \\ &= (e_{4,1}^{(\alpha)} \otimes \mathbb{I}_2)(\mathbb{I}_2 \otimes (\mathbb{I}_2 + i\mu\nu\sigma_z) + \sigma_x \otimes (\mu\sigma_x + \nu\sigma_y))(e_{4,1}^{(\beta)} \otimes \mathbb{I}_2) \\ &= e_{4,1}^{(\alpha)} e_{4,1}^{(\beta)} \otimes (\mathbb{I}_2 + i\mu\nu\sigma_z) + e_{4,1}^{(\alpha)} \sigma_x e_{4,1}^{(\beta)} \otimes (\mu\sigma_x + \nu\sigma_y) \\ &= \begin{cases} e_{4,1}^{(\alpha)} \otimes (\mathbb{I}_2 + i\mu\nu\sigma_z), & \alpha = \beta \\ e_{3,2}^{(\alpha)} \otimes (\mu\sigma_x + \nu\sigma_y), & \alpha \neq \beta \end{cases}. \end{aligned} \quad (4.7)$$

This gives all possible outcomes of the projection sequence and from before at least one of these is a braiding, so it remains to check the other outcomes for braiding. To do this lets look at the form of the braiding operator when applied after the initial projection,

$$U_{14}^{(\pm)} \Pi_{23}^{(\alpha)} = \exp\left(\pm i \frac{\pi}{4} \mathbb{I}_2 \otimes \sigma_z\right)(e_{4,1}^{(\alpha)} \otimes \mathbb{I}_2) = e_{4,1}^{(\alpha)} \otimes (\mathbb{I}_2 \pm i\sigma_z). \quad (4.8)$$

Therefore the projection sequence above gives a $U_{14}^{(\mu\nu)}$ braiding whenever $\alpha = \beta$. That is, to achieve braiding only one condition is imposed on the outcome of the projection sequence, which is that the initial and final outcome must be the same. Therefore for this projection sequence, the probability to achieve a braiding is clearly 50%. However, if one looks at the two distinct braidings, it is clear that the type of braiding depends on the outcome of the intermediate projections. So assuming that braiding has been achieved, it is equally likely that the braiding is clockwise or counter-clockwise. When the two intermediate measurements have the same outcome the result is a clockwise braiding, and counter-clockwise for opposite outcomes. One can easily check that this result is the same as that in Fig.4.1.

One can see that although this method greatly reduces the number of calculations, it does not provide any intuition or more general results about any other projection sequence. For this reason one again looks at this same projection sequence, this time

using the language of anyon models, with the goal of gaining some more general results about the action of projection sequences.

4.1.1 Anyon Models for Two-Sequences

The first generalisation is to relabel the MZMs γ_i by some general anyon label a_i since the anyon model rules apply more generally—later the results will again be restricted to MZMs for comparison purposes.

Using the representation of the projection operators in (2.24) the projection sequence—which will now be denoted $S_{12,24} = \Pi_{23}^{(b'_{23})} \Pi_{24}^{(b_{24})} \Pi_{12}^{(b_{12})} \Pi_{23}^{(b_{23})}$ —becomes,

$$S_{12,24} = \begin{array}{c} a_1 \quad a_2 \quad a_3 \quad a_4 \\ \begin{array}{c} \text{Diagram 1: A sequence of four vertices. Top vertex D (blue) has incoming lines from } a_2 \text{ (red) and } a_3 \text{ (red), and outgoing lines to } a_1 \text{ (blue) and } a_4 \text{ (blue). Below D is vertex B' (blue) with incoming lines from } a_2 \text{ (red) and } a_3 \text{ (red), and outgoing lines to } a_1 \text{ (blue) and } a_4 \text{ (blue). Below B' is vertex B (blue) with incoming lines from } a_2 \text{ (red) and } a_3 \text{ (red), and outgoing lines to } a_1 \text{ (blue) and } a_4 \text{ (blue). Bottom vertex C (blue) has incoming lines from } a_2 \text{ (red) and } a_3 \text{ (red), and outgoing lines to } a_1 \text{ (blue) and } a_4 \text{ (blue).} \end{array} \\ a_1 \quad a_2 \quad a_3 \quad a_4 \end{array} = \begin{array}{c} a_1 \quad a_2 \quad a_3 \quad a_4 \\ \begin{array}{c} \text{Diagram 2: A sequence of four vertices. Top vertex D (blue) has incoming lines from } a_2 \text{ (red) and } a_3 \text{ (red), and outgoing lines to } a_1 \text{ (blue) and } a_4 \text{ (blue). Below D is vertex B' (blue) with incoming lines from } a_2 \text{ (red) and } a_3 \text{ (red), and outgoing lines to } a_1 \text{ (blue) and } a_4 \text{ (blue). Below B' is vertex B (blue) with incoming lines from } a_2 \text{ (red) and } a_3 \text{ (red), and outgoing lines to } a_1 \text{ (blue) and } a_4 \text{ (blue). Bottom vertex C (blue) has incoming lines from } a_2 \text{ (red) and } a_3 \text{ (red), and outgoing lines to } a_1 \text{ (blue) and } a_4 \text{ (blue).} \end{array} \\ a_1 \quad a_2 \quad a_3 \quad a_4 \end{array} \quad (4.9)$$

The vertices which are going to be manipulated have been labelled and certain charge lines have been coloured so that the manipulations are easier to follow. The first manipulation has only used the fact that at vertex **D** it does not matter which way the incoming anyons fuse (2.13), so a_2 and a_3 have been allowed to switch places. The second equality is obtained using isotropy invariance and (2.8), that is the charge lines have been moved around without crossing vertices, and those that have changed orientation are replaced with their anti-particle. Then again using isotropy invariance, the Yang-Baxter relation

4.1 A Single Pairwise Projection Sequence

(2.29) and the F-move defined in (2.21) gives (for more details see Appendix.C),

$$S_{12,24} = \text{Diagram} \quad . \quad (4.10)$$

In the above \mathbf{A}' and \mathbf{B}' vertices are moved along the blue and red charge lines to join the \mathbf{B} and \mathbf{A} vertices giving rise to the new fusion line $g = b_{12} \times \bar{b}_{24}$. In order to make sure the diagram obeys the fusion rules the $a_5 = a_4 \times a_2 \times a_3$ charge was introduced, this is a consequence of the \mathbf{B}' having to move passed the \mathbf{C} and \mathbf{D} vertices using F-moves. Note that the phase and normalisation factors have been neglected, for full details see Appendix.C.

Now, within the framework of anyon models, the diagrams do not have to be unitary, but as mentioned in Sec.2.2, to meet the physical constraints of the system the diagrams are required to be unitary. In order for the above diagram to remain unitary all the b charges must be Abelian. This restricts the discussion from all possible anyon models to anyon models which are not strictly non-Abelian, such as the Ising (which will be discussed later in this chapter) and \mathbb{Z}_N -parafermion models. Thus one cannot use a model such as the Fibonacci anyon model where the only non-trivial anyon is non-Abelian. Details and definitions of the above anyon models can be found in [Bonderson and Preskill \[23\]](#). Now using the 2-2 F-move defined in (2.22) on the red part of the above diagram gives (more details can be found in Appendix.C),

$$S_{12,24} = \text{Diagram} \quad , \quad (4.11)$$

4.1 A Single Pairwise Projection Sequence

where $h = \bar{b}_{23} \times b'_{23}$. This diagram uncovers a fact already confirmed in the previous calculations, that is the initial and final projections must have the same outcome ($b_{23} = b'_{23}$) in order to achieve braiding. If the outcomes are not the same then one always has the extra charge line h which destroys the braiding (which matches the results in Fig.4.1 and (4.7)). Let's now consider the case when the outcomes are the same, this allows us to remove the h line since it becomes the vacuum charge, and hence completely dissociate the two parts of the diagram it connects. In this situation the diagram involving a_2 and a_3 is just a projection so one has the following,

$$S_{12,24} = \Pi_{23}^{(b'_{23})} \Pi_{24}^{(b_{24})} \Pi_{12}^{(b_{12})} \Pi_{23}^{(b_{23})} = \hat{X}_{14} \otimes \Pi_{b_{23}}^{(23)}, \quad (4.12)$$

where \otimes represents the fact that the diagrams are simply placed “on top” of one another—thus are dissociated—and \hat{X}_{14} represents the part of the diagram containing the braiding, using (2.28) gives,

$$\hat{X}_{14} = \begin{array}{c} \begin{array}{cc} a_1 & a_4 \\ & \diagdown \quad \diagup \\ & \times \\ & \diagup \quad \diagdown \\ a_1 & a_4 \end{array} \\ \\ \begin{array}{cc} a_1 & a_4 \\ & \diagup \quad \diagdown \\ & \times \\ & \diagdown \quad \diagup \\ a_1 & a_4 \end{array} \end{array} = \sum_c R_c^{a_4 a_1} \begin{array}{c} \begin{array}{cc} a_1 & a_4 \\ & \diagdown \quad \diagup \\ & \times \\ & \diagup \quad \diagdown \\ a_1 & a_4 \end{array} \\ \\ \begin{array}{cc} a_1 & a_4 \\ & \diagup \quad \diagdown \\ & \times \\ & \diagdown \quad \diagup \\ a_1 & a_4 \end{array} \end{array}. \quad (4.13)$$

Using a single 2-2 F-move and (2.16) \hat{X}_{14} can be reduced to (see Appendix.C),

$$\hat{X}_{14} = \sum_c [F_c^{a_4 g a_4}]_{a_1 a_1} R_c^{a_4 a_1} \begin{array}{c} \begin{array}{cc} a_1 & a_4 \\ & \diagdown \quad \diagup \\ & \times \\ & \diagup \quad \diagdown \\ a_1 & a_4 \end{array} \\ \\ \begin{array}{cc} a_1 & a_4 \\ & \diagup \quad \diagdown \\ & \times \\ & \diagdown \quad \diagup \\ a_1 & a_4 \end{array} \end{array} = \sum_c [F_c^{a_4 g a_4}]_{a_1 a_1} R_c^{a_4 a_1} \Pi_{14}^{(c)}. \quad (4.14)$$

Therefore \hat{X}_{14} is a modified braiding, the orientation of which depends on $g = b_{12} \times \bar{b}_{24}$. In order to apply this result to the system of MZMs in Fig.3.1, one requires the anyon model that describes MZMs, that is the fusion category, braiding category and the set of particle types involved in fusion of MZMs. The model is the Ising anyon model which is described in Table.4.1 or for a pictorial representation one can look to [26]. The non-Abelian anyons in the Ising model are the σ anyons, which represent the MZMs. I

4.1 A Single Pairwise Projection Sequence

Ising Anyon Model

$\mathcal{C} = \{I, \sigma, \psi\}, \quad d_I = d_\psi = 1, \quad d_\sigma = \sqrt{2}$
$\sigma \times \sigma = I + \psi, \quad I \times a = a \times I = a, \quad \sigma \times \psi = \psi \times \sigma = \sigma, \quad \psi \times \psi = I$
$R_I^{\sigma\sigma} = e^{-i\pi/8}, \quad R_\psi^{\sigma\sigma} = e^{i3\pi/8}, \quad R_I^{\psi\psi} = -1, \quad R_\sigma^{\sigma\psi} = R_\sigma^{\psi\sigma} = -i$
$[F_\psi^{\sigma\psi\sigma}]_{\sigma\sigma} = [F_\sigma^{\psi\sigma\psi}]_{\sigma\sigma} = -1, \quad [F_\sigma^{\sigma\sigma\sigma}]_{ef} = \frac{1}{\sqrt{2}} \begin{pmatrix} 1 & 1 \\ 1 & -1 \end{pmatrix}_{ef}$

Table 4.1 Ising Anyon Model: where $a \in \mathcal{C}$ and $e, f \in \{I, \psi\}$. The first row contains the set of particles and the values of the quantum dimension. The second row is the fusion rules of each of the particles. Then the final two rows give the phases picked up under R -moves and F -moves. All the non-trivial F -moves and R -moves are listed. Any other F -move or R -move allowed by the fusion rules above are unity and vanish otherwise. The final F -move is a matrix, this is not used in this thesis but more information can be found in [26].

and ψ represent the empty and filled state of a fermion, thus the fusion rule $\sigma \times \sigma = I + \psi$ represents the fact that when one combines two MZMs they form an unoccupied or occupied fermion mode.

Applying the Ising model to (4.9) for the wire set-up in Fig.3.1, all the MZMs are represented by σ anyons, that is $a_1 = a_2 = a_3 = a_4 = \sigma$. All the b anyons are either the vacuum anyon I or the fermion ψ . Then (4.14)—note that the initial and final outcomes are still assumed to be the same—has two possible outcomes. The first is when $g = b_{12} \times \bar{b}_{24} = I$, in which case when $b_{12} = b_{24}$ then $\hat{X}_{14} = R_{\sigma\sigma}$, up to a phase. This corresponds to a clockwise braiding of the MZMs. The second outcome is $\hat{X}_{14} = R_{\sigma\sigma}^{-1}$, which corresponds to $b_{12} \neq b_{24} \Rightarrow g = b_{12} \times \bar{b}_{24} = \psi$, which is a counter-clockwise braiding. This matches the results of the previous calculations, although it was more difficult to reach them in this manner it is much easier to generalise from this method. This is the goal of Sec.4.2 and Sec.4.3.

Before continuing, one must also calculate the probability of achieving a braiding. This is of course 50% since half of the outcomes of the sequence $S_{12,24}$ lead to a braiding. So it only remains to check that at each stage the fusion of the two MZMs in the projection has an equal chance of each outcome. This implies that one achieves counter-clockwise and clockwise braidings with equal probability. This is most easily seen using anyon models. Each fusion of two anyons has a probability associated with each possible outcome which is related to the quantum dimension of the anyon defined in (2.9) [34]. For in the Ising model, the fusion of two σ anyons— $\sigma \times \sigma = a$ for $a \in \{I, \psi\}$ —has probability $d_a/d_\sigma d_\sigma$, but using Table.4.1 each a has quantum dimension $d_a = 1$. Thus both are equally likely and, therefore, so are the clockwise and counter-clockwise braidings.

This approach has reaffirmed the results of Fig.4.1 and (4.7) for MZMs. However since the anyon model method is not restricted to MZMs, the results here apply more generally. That is, some of the results also apply to *any* not strictly non-Abelian anyon model. In particular, if one performs a two-sequence of projections in a not strictly non-Abelian anyon model, in order for a braiding to occur it must be the case that the initial and final projections have the same outcome (which must be Abelian). However, the results attained from using the Ising anyon model need not hold in general. Namely the condition relating the orientation of the braiding (clockwise or counter-clockwise) to the outcome of the intermediate projections. Also it need not be the case that each outcome of a projection operator in other anyon models be equally likely. This may lead to one of the orientations of braiding being favoured in another not strictly non-Abelian anyon model.

4.2 Topological Symmetries of Two-Sequences

Now that it has been shown that this sequence of projections results in a braiding, the next step is to investigate what other sequences also gives a braiding and see if one can find the requirements for this to occur.

Let's begin by using the fact that the problem of counting the number of pairwise projections between n MZMs is the same as counting the number of ways to draw a line between n dots, so there are $n(n-1)/2$ possible pairwise projections. Thus for the set-up under consideration there are only 6 possible projections. However, since projections square to the identity, repeating the same projection twice in a row is trivial. This reduces the number of possible projections to 5. Therefore, by simple combinatorics there are $({}^5C_1)({}^4C_1) = 20$ possible sequences. Although one can impose one more restriction, that is not using the trivial projection $\Pi^{(14)}$ if one wants to perform a U_{14} braiding it is not immediately clear from the anyon model approach that this will destroy any chance of achieving a braiding—however an argument based on the trajectories of the anyons that explains why this is true is given in Fig.4.4. In the meantime consider the following hand-wavy spin algebra calculation as motivation for why this is the case. The projection has the form,

$$\Pi_{14}^{(\mu)} = 1 + i\gamma_1\gamma_4 = \mathbb{I}_4 + i\mu(\mathbb{I}_2 \otimes \sigma_x)(\mathbb{I}_2 \otimes \sigma_y) = \mathbb{I}_2 \otimes (\mathbb{I}_2 - \mu\sigma_z) = \mathbb{I}_2 \otimes e_{4,1}^{(\mu)}, \quad (4.15)$$

therefore one cannot achieve a braiding since there is a unit matrix on the RHS of the tensor product, and multiplying this with other projections will result in a linear

4.2 Topological Symmetries of Two-Sequences

combination of unit matrices tensored together. This takes away another possible projection from the count above. Therefore the number reduces to $({}^4C_1)({}^3C_1) = 12$ projection sequences. The set of possible projections is $\mathfrak{P} = \{\Pi_{34}, \Pi_{24}, \Pi_{13}, \Pi_{12}\}$.

Using the diagrams, it is clear that if only two projections are used in the sequence then they must involve the MZMs to be braided. For example, for the U_{14} braiding one needs the intermediate projections to be of the form $\Pi_{a_4} \in \mathfrak{P}$ and $\Pi_{1b} \in \mathfrak{P}$. From looking at some example diagrams it is clear why this condition is necessary but not sufficient to achieve the desired braiding. Consider the projection sequence $\Pi_{b'_{23}}^{(23)} \Pi_{b_{24}}^{(24)} \Pi_{b_{34}}^{(34)} \Pi_{b_{23}}^{(23)}$, diagrammatically:

$$\Pi_{b'_{23}}^{(23)} \Pi_{b_{24}}^{(24)} \Pi_{b_{34}}^{(34)} \Pi_{b_{23}}^{(23)} = \begin{array}{c} a_1 \ a_2 \ a_3 \ a_4 \\ \begin{array}{c} \text{Diagram showing the braiding of } a_1, a_2, a_3, a_4 \text{ with projections } b'_{23}, b_{24}, b_{34}, b_{23} \end{array} \\ a_1 \ a_2 \ a_3 \ a_4 \end{array} . \quad (4.16)$$

It is clear here that the a_1 anyon is unaffected by the projections. This demonstrates the necessity of having projections of the form discussed above. To show that this is not sufficient consider the following projection sequence $\Pi_{23}^{(b'_{23})} \Pi_{34}^{(b_{34})} \Pi_{12}^{(b_{12})} \Pi_{23}^{(b_{23})}$, diagrammatically:

$$\Pi_{23}^{(b'_{23})} \Pi_{34}^{(b_{34})} \Pi_{12}^{(b_{12})} \Pi_{23}^{(b_{23})} = \begin{array}{c} a_1 \ a_2 \ a_3 \ a_4 \\ \begin{array}{c} \text{Diagram showing the braiding of } a_1, a_2, a_3, a_4 \text{ with projections } b'_{23}, b_{34}, b_{12}, b_{23} \end{array} \\ a_1 \ a_2 \ a_3 \ a_4 \end{array} . \quad (4.17)$$

This diagram uses red lines to make the middle two projections of this sequence more discernible. Notice that when one isolates this part of the diagram there is no connection between the a_1 and a_4 anyons and therefore there can be no braiding between them. This

4.3 Topological Symmetries of Three-Sequences

illustrates the fact that the previous condition—hereafter referred to as the connection condition—is necessary but not sufficient to braid the anyons. This leaves 4 of the 12 possible sequences discussed earlier.

One has already been discussed and Fig.4.2 argues that using symmetries of the Ising model that all of four lead to the same results (the symmetries in Fig.4.2 will be referred to as rotation and inversion symmetries). That is, in the situation where one sequence results in a clockwise braiding, then one of the other three will also result in a clockwise and the remaining two will result in a counter-clockwise braiding. The argument uses the fact that Ising anyons are all self-dual, that is they are their own unique counterpart anyons, which fuse to the identity. This fact is represented in the fusion rules of Table.4.1.

Since the connection condition was derived in terms of general anyon model theory, it holds for any anyon model, not just the Ising model. That is, to braid two anyons, α and β , through a two-sequence of projections, it is necessary that the two intermediate projections have the form $\Pi_{\alpha\theta}$ and $\Pi_{\beta\theta}$, where θ is another anyon in the same model. However, the inversion and rotation symmetry only apply to anyon models in which each anyon is self-dual.

4.3 Topological Symmetries of Three-Sequences

This section will investigate the increased number of projections as it is the simplest extension of the previous work with two projections. Consider three-sequences (three intermediate projections instead of two) and start as before with the case of two-sequences, identify the number of different sequences and find symmetries between them to lighten the load of calculation. The same minimal set-up is used so the number of projections is the same, that is there are 6 distinct projections. Moving to a higher number projections removes some of the restrictions imposed by the two projection case. The first is the ability to repeat measurements as long another projection is performed in-between. So including the fact that one must not want to perform the Π_{14} projection and also that one does not want to repeat the initial and final projection Π_{23} as the first or third measurement, leaves $({}^4C_1)({}^5C_1)({}^4C_1) = 80$ total possible sequences. However the above count includes sequences which perform the same projection in succession, so removing these one is left with $({}^4C_1)({}^3C_1)({}^3C_1) + ({}^4C_1)({}^4C_1) = 52$.

One can begin to manifest the symmetries of the system by first choosing a first projection and each possible sequence for that projection, then removing the sequences covered by some symmetry argument. Fig.4.3 shows all the three-sequences which start with Π_{12} as the first projection, excluding all sequences which do not satisfy the

Symmetries in Ising Anyon Model Projection Sequences

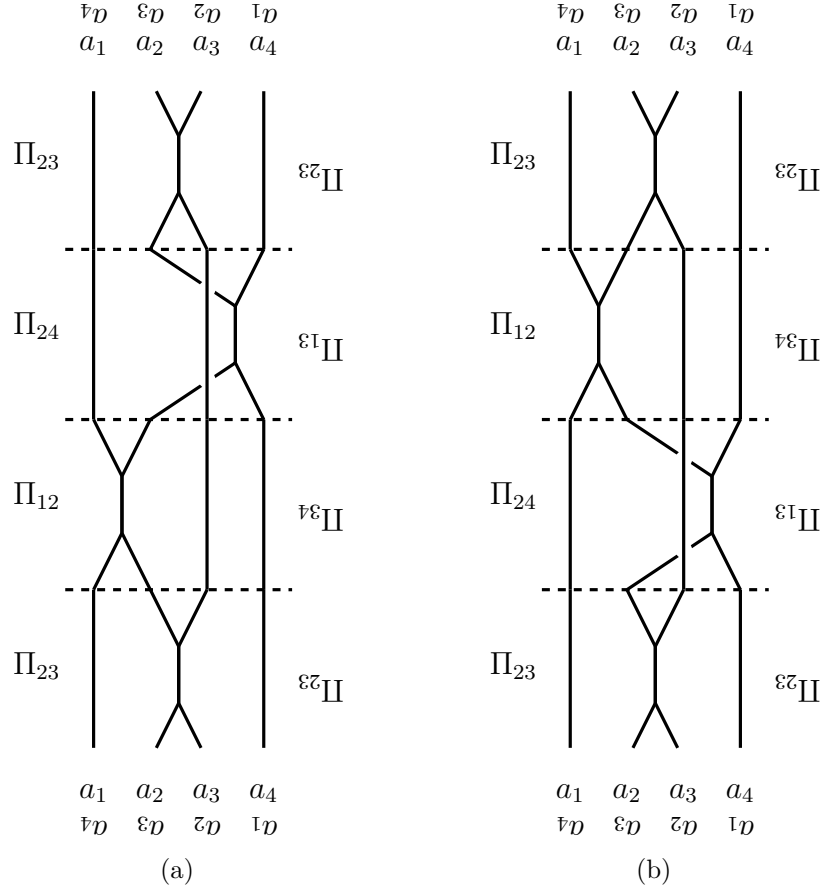


Fig. 4.2 (a) and (b) are the diagrammatic representations of the projection sequences $\Pi_{23}\Pi_{24}\Pi_{12}\Pi_{23}$ and $\Pi_{23}\Pi_{12}\Pi_{24}\Pi_{23}$ respectively. The purpose of this figure is to show that on rotating the diagrams by 180° (turning the page upside down), the above diagrams are in fact also representations of the sequences $\Pi_{23}\Pi_{34}\Pi_{13}\Pi_{23}$ and $\Pi_{23}\Pi_{12}\Pi_{24}\Pi_{23}$ when the arrows (which are omitted) are reversed, that is the anyons are replaced by their dual. This thesis is mainly concerned with the Ising anyon model (since it is the model that describes MZMs) in which every anyon is self-dual. Therefore, on rotation of the diagrams the result of the sequences is simply the inverse of the result of the non-rotated diagram. The other symmetry that should be noted here is that if one reflects the diagram in (a) in the horizontal axis from above or below the diagram and again reversing the arrows orientation the result is the same as the diagram in (b). That is, under this symmetry $\Pi_{23}\Pi_{24}\Pi_{12}\Pi_{23}$ goes to $\Pi_{23}\Pi_{12}\Pi_{24}\Pi_{23}$ and vice versa. Alternatively to see this symmetry one could place (a) “on top” of (b) and notice that they are mirror images with inversed arrow orientations. Thus if one of the sequences results in a braiding the other three do also.

4.3 Topological Symmetries of Three-Sequences

connection condition from (4.17), which in the pictorial terms of Fig.4.3 means they do not have some arrow pathway between the two dots. This condition removes 16 total sequences leaving 36 sequences.

Now the diagram symmetry from Fig.4.2 implies that for every sequence there are three other sequences which also lead to the “same” result. Therefore, one is left with 9 unique sequences. In fact, these 9 sequences are exactly those from Fig.4.3. One can see this by noting the action of the rotation and inversion symmetries on the pictorial diagrams of Fig.4.3. Inversion that is the mirror symmetry from Fig.4.2, exchanges the first and third projections of the sequence.

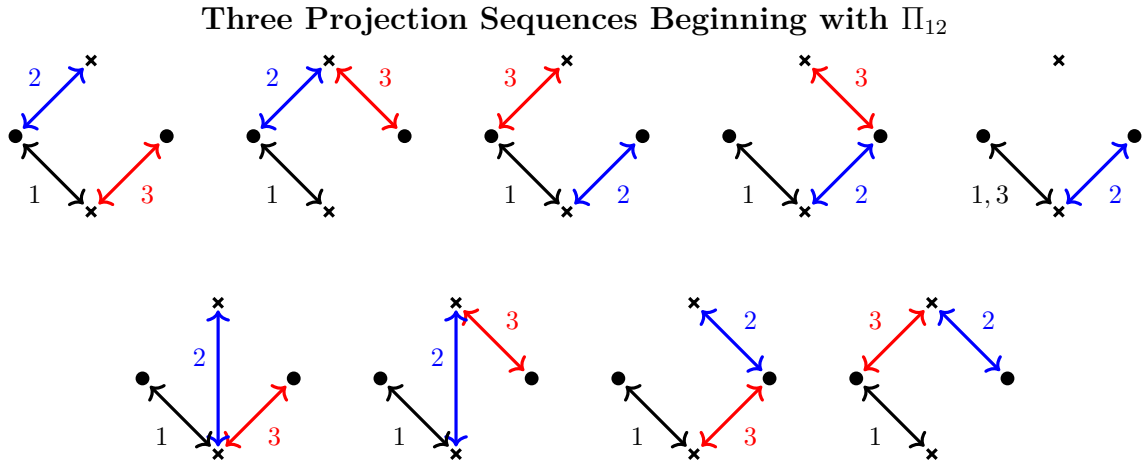


Fig. 4.3 Exhaustive list of three projection sequences beginning with Π_{12} . Projections are represented as double arrowed numbered lines, where the numbers and colours represent the order in the sequence. The crosses and dots represent Majorana which are ancillary and computational respectively.

The rotation symmetry rotates each of the arrows 180° preserving the order. From these two symmetries one can manipulate the diagrams in Fig.4.3 to achieve any of the 36 possible sequences.

All that remains is to investigate each of these 9 sequences, this thesis will consider one sequence and uses the anyon model diagrams to argue that one cannot achieve a braiding in the three-sequence case (other than the trivial extension of the two-sequence case). The argument is as follows, suppose one takes the sequence $\Pi_{23}\Pi_{34}\Pi_{23}\Pi_{12}\Pi_{23}$ and finds the paths from a_1 to a_4 and from a_4 to a_1 , as shown in Fig.4.4. Then a braiding is only possible if one can manipulate the diagram such that the two paths cross each other, and all other charge lines connecting the paths are trivial for some measurement outcome or can be manipulated away using F-moves. Fig.4.4 shows an example of these paths for a three-sequence and for a two-sequence. The eight remaining independent

Anyon Trajectories in Projection Sequences

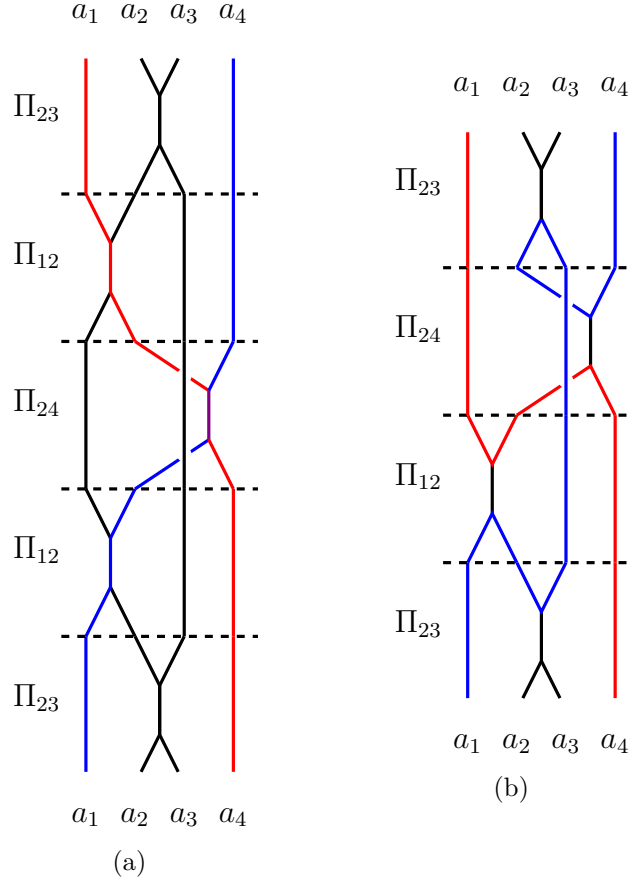


Fig. 4.4 The trajectories in these diagrams represent possible pathways from a_1 to a_4 (blue line) and from a_4 to a_1 (red line). (b) shows a two projection sequence in which is possible to find two trajectories that do not pass through the same charge line and also cross each other. If a diagram does not meet these conditions it cannot form a U_{14} braiding, for example (a) cannot form a braiding since the red and blue trajectories must pass through the purple charge line. One can find other trajectories in this sequence that do not intersect at this point but the lines must always intersect. This means one cannot form a braiding because there is no way to manipulate the two trajectories such that they resemble a braiding diagram, that is cross each other with charge lines connected them that are trivial in certain cases of measurement outcome. Note that if one uses the Π_{14} projection that the trajectories are forced to pass through a single charge line. Thus including Π_{14} in a sequence destroys the chance of braiding (a fact that was used in Sec.4.2).

sequences can be found in Appendix.D, upon investigation of the charge line trajectories, it is clear that none of these can form a braiding. This can be checked using the spin algebra from Sec.4.1.

This closes the case of three-sequences, one cannot achieve a braiding in a non-trivial way. The next step would be to either increase the number of projections or to increase the number of qubits (pairs of MZMs), however the discussion of these is left to Sec.5.1.

4.4 Measurement Protocol & Experimental Realisation

4.4.1 Measurement Protocol

Suppose one chooses to use the sequence $\Pi_{23}^{(\beta)} \Pi_{24}^{(\mu)} \Pi_{12}^{(\nu)} \Pi_{23}^{(\alpha)}$ and particularly wants to perform a counter-clockwise braiding on the system. Then from Fig.4.1, the two intermediate projections must have the opposite outcome, that is $\mu = -\nu$. But these outcomes are inherently probabilistic, so if an undesirable outcome is achieved on the first measurement of Π_{24} , how does one acquire the counter-clockwise braiding? The answer is simply repeat the previous measurement Π_{12} and then apply Π_{24} again. This process can be repeated until the desired outcome is achieved. Consider the following diagram as a manifestation of the protocol,

$$\begin{array}{c}
 a_1 \ a_2 \ a_3 \ a_4 \\
 \Pi_{24} \\
 \text{---} \\
 \Pi_{12} \\
 \text{---} \\
 \Pi_{24} \\
 \text{---} \\
 \Pi_{12} \\
 a_1 \ a_2 \ a_3 \ a_4
 \end{array}
 =
 \begin{array}{c}
 a_1 \ a_2 \ a_3 \ a_4 \\
 \Pi_{24} \\
 \text{---} \\
 \Pi_{12} \\
 a_1 \ a_2 \ a_3 \ a_4
 \end{array}
 \quad (4.18)$$

Using isotropy invariance one can “contract” the a_4 charge line so that the four projections on the LHS are equal to performing the two on the right. One can of course repeat this

4.4 Measurement Protocol & Experimental Realisation

process at any point in the sequence, including on the final projection (which must have the same outcome as the initial projection to achieving a braiding). This protocol allows one to attain the desired result (up to an unimportant phase factor) with 100% certainty. The only uncertainty in the protocol is the number of times the process will need to be repeated to achieve the desired outcome, and also whether the protocol will have to be repeated for multiple projections in the sequence.

It is a basic fact of probability theory that, since each measurement is independent, and each outcome is equally likely, the probability of the desired outcome being achieved on the n -th iteration of the protocol $P(n)$ is a geometric series,

$$P(n) = \sum_{k=1}^n \left(\frac{1}{2}\right)^k = 1 - 2^{-n}. \quad (4.19)$$

Looking at the equation and its graph (Fig.4.5), it is clear that the probability of success grows exponentially with number of iterations. Similar protocols have been developed by [Bonderson et al. \[16\]](#) and [Vijay and Fu \[35\]](#).

Measurement Iteration Protocol Probability Plot

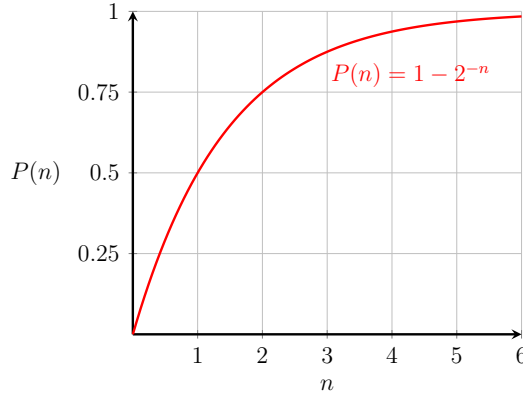


Fig. 4.5 The diagram shows the probability of achieving the desired braiding (clockwise or counter-clockwise) for the sequence of projections, say $\Pi_{23}\Pi_{12}\Pi_{24}\Pi_{23}$, as a function of the number of iterations of the protocol n . That is, the number of times $\Pi_{12}\Pi_{24}$ are repeated until the desired outcome is achieved. The probability function is a geometric series and so grows exponentially with $P(n) \rightarrow 1$ as $n \rightarrow \infty$.

4.4.2 Experimental Realisation

The final section of this chapter is dedicated to finding a way to experimentally perform the projective measurements. The measurement scheme is adapted from that of [Romito and Gefen \[27\]](#), which measures the charge of weakly tunnel-coupled quantum dots (QDs)

4.4 Measurement Protocol & Experimental Realisation

which are coupled to the Majorana junction in Fig.3.1. Although in the above paper uses four QDs coupled to 6 MZMs, here one actually still needs four QDs to connect to the 4 MZMs in order to be able to perform all possible projections. The set-up is shown in Fig.4.6.

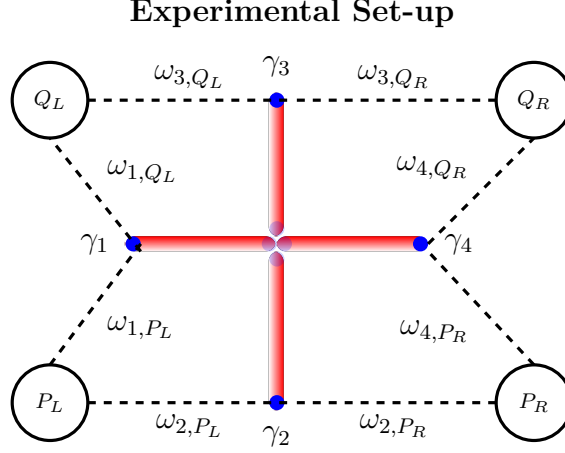


Fig. 4.6 The multi-terminal junction of one dimensional nanowires (red lines) hosting MZMs at the ends (blue dots), designed in such a way that each of the MZMs in the center (the faded blue dots) pair up. Leaving four unpaired MZMs labelled by $\gamma_1, \dots, \gamma_4$. The measurement apparatus is split into two sections denoted L & R . The black circles represent quantum dots (labelled by P_a and Q_b where $a, b \in \{L, R\}$) which are weakly coupled to the MZMs by tunnelling-couplings (black dashed lines) of strength $\omega_{\alpha,\beta}$ (where $\alpha \in \{1, 2, 3, 4\}$ and $\beta \in \{Q_L, Q_R, P_L, P_R\}$).

As in [27] the QDs are tuned so that on the energy scales considered only one orbital is relevant. The electron annihilation operator of this level in the P_L QD is denoted c_{P_L} and similarly for the fermionic operators of the other QDs. The charge configuration of the QDs can then be measured and the tunnelling strength $\omega_{\alpha,\beta}$ which could be time dependent is controlled. Romito and Gefen [27], and references, therein explain how to experimentally perform the above.

The detector Hamiltonian for the left side of the system is,

$$\begin{aligned} \mathcal{H}_L = & \omega_{3,Q_L}(c_{Q_L}^\dagger - c_{Q_L})\gamma_3 + \omega_{1,Q_L}(c_{Q_L}^\dagger - c_{Q_L})\gamma_1 \\ & + \omega_{1,P_L}(c_{P_L}^\dagger - c_{P_L})\gamma_1 + \omega_{2,P_L}(c_{P_L}^\dagger - c_{P_L})\gamma_2. \end{aligned} \quad (4.20)$$

Suppose that the left side of the system is initialised in the state $|\psi_0\rangle = q_L|1,0\rangle + p_L|0,1\rangle = (q_L c_{Q_L}^\dagger + p_L c_{P_L}^\dagger)|0\rangle_L$ where $|0\rangle_L$ denotes the vacuum of the QDs on the left. The state is also normalised such that $|q_L|^2 + |p_L|^2 = 1$. Now suppose that the tunnel-couplings are switched on for a finite time Δt , then after this time has elapsed the state

4.4 Measurement Protocol & Experimental Realisation

becomes,

$$\begin{aligned} |\psi_{L,(n_{Q_L},n_{P_L})}\rangle &= (c_{Q_L}^\dagger c_{Q_L})^{n_{Q_L}} (c_{Q_L} c_{Q_L}^\dagger)^{1-n_{Q_L}} (c_{P_L}^\dagger c_{P_L})^{n_{P_L}} (c_{P_L} c_{P_L}^\dagger)^{1-n_{P_L}} \\ &\cdot \exp(-i\mathcal{H}_L \Delta t) |\psi_0\rangle. \end{aligned} \quad (4.21)$$

Where $n_{Q_L}, n_{P_L} \in \{0, 1\}$ are the number of electrons in the Q_L and P_L QDs. Now considering the weak measurement limit, then for finite Δt one can expand the time evolution operator $\exp(-i\mathcal{H}_L \Delta t)$ to second order in Δt (one could also consider the strong measurement limit for small Δt),

$$\exp(-i\mathcal{H}_L \Delta t) \approx 1 - \frac{(\Delta t)^2}{2} (\eta + i\lambda \hat{O}_L (c_{Q_L} c_{P_L}^\dagger - c_{P_L} c_{Q_L}^\dagger)). \quad (4.22)$$

Where

$$\begin{aligned} \eta &= \frac{1}{2} (\omega_{3,Q_L}^2 + \omega_{1,Q_L}^2 + \omega_{1,P_L}^2 + \omega_{2,P_L}^2), \\ \lambda &= \omega_{1,P_L}^2 \omega_{3,Q_L}^2 + \omega_{1,Q_L}^2 \omega_{2,P_L}^2 + \omega_{3,Q_L}^2 \omega_{2,P_L}^2, \\ \hat{O}_L &= \frac{-i}{\lambda} (\omega_{1,Q_L} \omega_{2,P_L} \gamma_1 \gamma_2 + \omega_{3,Q_L} \omega_{1,P_L} \gamma_3 \gamma_1 + \omega_{3,Q_L} \omega_{2,P_L} \gamma_3 \gamma_2). \end{aligned} \quad (4.23)$$

Applying this approximation to (4.21) with the QD charge configuration $n_{Q_L} = 1, n_{P_L} = 0$ gives,

$$|\psi_{L,(1,0)}\rangle = (c_{Q_L}^\dagger c_{Q_L}) (c_{P_L} c_{P_L}^\dagger) \left(1 - \frac{(\Delta t)^2}{2} (\eta + i\lambda \hat{O}_L (c_{Q_L} c_{P_L}^\dagger - c_{P_L} c_{Q_L}^\dagger)) \right) |\psi_0\rangle. \quad (4.24)$$

Expanding this out,

$$\begin{aligned} |\psi_{L,(1,0)}\rangle &= \left(1 - \frac{(\Delta t)^2}{2} \eta \right) (c_{Q_L}^\dagger c_{Q_L}) (c_{P_L} c_{P_L}^\dagger) |\psi_0\rangle \\ &\quad - i \frac{\lambda (\Delta t)^2}{2} \hat{O}_L (c_{Q_L}^\dagger c_{Q_L}) (c_{P_L} c_{P_L}^\dagger) (c_{Q_L} c_{P_L}^\dagger - c_{P_L} c_{Q_L}^\dagger) |\psi_0\rangle, \\ |\psi_{L,(1,0)}\rangle &= \left(q_L \left(1 - \frac{(\Delta t)^2}{2} \eta \right) + i p_L \frac{\lambda (\Delta t)^2}{2} \hat{O}_L \right) |1, 0\rangle. \end{aligned} \quad (4.25)$$

Now the form of a projection operator, up to a phase, is $\Pi_{ab}^{(-)} = 1 - i\mu\gamma_a\gamma_b$, thus for the above to be a projection one can tune the tunnel-couplings and then perform the charge measurement for a certain time. For example, if one wants to measure the Π_{12} , then the

4.4 Measurement Protocol & Experimental Realisation

tunnelling coupling ω_{3,Q_L} must vanish and the following must hold,

$$q_L \left(1 - \frac{(\Delta t)^2}{2} \eta \right) = i p_L \lambda \frac{(\Delta t)^2}{2}, \quad \text{and} \quad |q_L|^2 + |p_L|^2 = 1. \quad (4.26)$$

Note that the above equation is dimensionless, so the time in dimensionless form $\sqrt{\eta} \Delta t$ can be written,

$$\sqrt{\eta} \Delta t = \sqrt{\frac{2q_L}{i p_L (\lambda/\eta) + q_L}} = \sqrt{\frac{2(|q_L|^2 - i(\lambda/\eta) \bar{p}_L q_L)}{|p_L|^2 (\lambda/\eta)^2 + |q_L|^2 + 2(\lambda/\eta) \text{Im}(p_L \bar{q}_L)}}. \quad (4.27)$$

The conditions for this time to be real are, $p_L \bar{q}_L$ is purely imaginary with $\text{Im}(p_L \bar{q}_L) \geq 0$ and $|q_L|^2 \geq i(\lambda/\eta) \bar{p}_L q_L$. This process can, of course, be replicated for the other projection operators of interest, and for the other side of the set-up.

Now that the method has been developed let's consider a specific example. Suppose again one wants to measure Π_{12} . First one would initialise the state (the simplest choice is $q_L = i p_L = 1/\sqrt{2}$) and the QD charge configuration, to say $n_{Q_L} = 1$, $n_{P_L} = 0$. Then tune the tunnelling couplings so that $\omega_{1,P_L} = \omega_{3,Q_L} = 0$ and $\omega_{1,Q_L} \omega_{2,P_L} = 1$. One can easily check that in this set-up one must switch on the couplings for the finite time $\sqrt{\eta} \Delta t = 1$, in order to perform the projection Π_{12} .

Chapter 5

Conclusion

The main aim of this thesis was to investigate the probabilistic nature of projection sequences that result in braiding of MZMs in Majorana-based TQC. With the goal of developing a method of manipulating the probabilities of a successful braiding so that one can better control the outcomes.

In order to begin investigating the above, one must first choose a model. Chap.3 introduces the minimal complexity model. It uses four MZMs, leading to a four-fold degenerate ground-state manifold, which allows the system to be used as a two-qubit system, one ancillary and one computational. A physical realisation of the set-up using a multi-terminal junction of four one-dimensional topological superconducting nanowires is also suggested (Fig.4.6).

Bonderson et al. [16] showed that the two-sequence $\Pi_{23}\Pi_{24}\Pi_{12}\Pi_{23}$ of MZMs resulted in a braiding under certain outcomes of the measurements. This sequence was investigated in Chap.4 using several mathematical formalisms: fermion algebra, spin algebra, and using anyon models. The goal was to determine the probability with which the conditions are met for each braiding orientation (clockwise or counter-clockwise), and also to look for generalisations. Using the fermion algebra it was found that, if the initial and final projection of the sequence must have the same outcome, then a braiding was attained. It was also shown that this is, in fact, the only necessary condition. Thus the probability of achieving a braiding is 50%. Each orientation of this braiding was found to be equally likely and determined by the outcome of the two intermediate projections. For clockwise braiding the outcomes must be the same and for a counter-clockwise braiding they must be distinct, these results are depicted in Fig.4.1. There is no obvious way to generalise these results, using this method or the spin algebra method.

A general anyon model allows one to define a projection without specifically stating the particle type. Thus, one can immediately generalise the above procedure to the

case of general anyons not just MZMs, this is done in Sec.4.1.1. Applying the same projection as above (but now for a general anyon) one finds that, in fact, only a not strictly non-Abelian anyon model can be used. One also finds that the initial and final outcome condition found for MZMs actually applies to all such anyon models, provided the outcomes of the projections are Abelian. This method, of course, also reaffirms the results of the previous calculations where the Ising anyon model is used.

When looking at general two-sequences the diagrammatic formalism of anyon models manifests some very subtle symmetries. The resulting symmetries impose conditions on the form of the intermediate projections and also show that every sequence has three isomorphic counterparts. That is, if one of the sequences results in a braiding, the three counterparts do also. Moving to the case of three-sequences the symmetries found for two-sequences still apply, and (with one additional argument) show that it is impossible to form a braiding which is a non-trivial extension of the two-sequence case. The one additional argument that was needed actually suggests that the situation will only deteriorate for higher order n -sequences, thus it is unlikely that braidings become more favoured probabilistically as one adds more intermediate projections.

Since the higher order cases are now assumed to be redundant, there are multiple ways to proceed, as discussed in Sec.5.1. This thesis returns to the two-sequence case in order to design a measurement protocol that will guarantee a braiding. The protocol takes advantage of the fact that the projection outcomes required to achieve a braiding are known. So when an undesired outcome occurs, the protocol corrects for this. The protocol is simply to repeat the previous measurement and then the measurement that gave the undesired outcome repeatedly until the desired outcome is achieved. This process is probabilistic only in the number of times that the process must be repeated. Although still probabilistic, the probability of not achieving a braiding is exponentially suppressed by the number of iterations.

The final part of the thesis deals with an experimental realisation of the projection measurements. The approach involves coupling quantum dots to the MZMs through tunnelling-couplings which are time dependent and controlled. The couplings are turned on for a finite time then the charge of the dots is measured. It was then shown how one can perform all of the possible projections using this method and thus perform a braiding through repeated application of this protocol.

5.1 Further Work

There are many areas for further research since there are many ways to generalise the work of this thesis. The first, and most obvious, is to increase the number of MZMs in the system. This gives more freedom when it comes to which projections to choose and may also enable the use of higher order sequences since there are more charge lines available, so the braiding anyons worldlines may not intersect.

The second builds on the first as it uses more MZMs but uses higher order projections such as the 3-projector defined in (2.25)—however for MZMs one must use an even order projector. The idea is the same as above one is increasing the charge lines may increase the probability that one can achieve a braiding. With this method, one also increases the possible number of charges of the subspace that one is projecting onto. Since a collection of 4 MZMs can have charge 0, 1 or 2, there is a possibility that this could increase the probability of favouring a certain braiding orientation since the number of measurement outcomes is increased.

It is known that MZMs cannot give fully topologically protected universal quantum computation, one needs to add some other non-topologically protected operations to achieve this. However parafermions can be used for universal quantum computation that is also topologically protected. So an obvious extension of this work is to apply the \mathbb{Z}_N -parafermion anyon model to the above results, however many of the symmetries used here do not carry over trivially hence the need for further work.

References

- [1] I. Chuang M. Nielsen. *Quantum computation and quantum information*. Cambridge University Press, New York, 2000. ISBN 0521632358.
- [2] R. Feynman. *Simulating physics with computers*. *International Journal of Theoretical Physics*, 21(6):467–488, Jun 1982. ISSN 1572-9575. doi: 10.1007/BF02650179. URL <https://doi.org/10.1007/BF02650179>.
- [3] P. Shor. *Fault-tolerant quantum computation*. 1996. ISSN 0272-5428. doi: 10.1109/SFCS.1996.548464. URL <http://arxiv.org/abs/quant-ph/9605011>.
- [4] S. B. Bravyi and A. Kitaev. *Fermionic quantum computation*. *Annals of Physics*, 298(1):210–226, 2002. ISSN 00034916. doi: 10.1006/aphy.2002.6254.
- [5] E. C. Rowell and Z. Wang. *Mathematics of Topological Quantum Computing*. pages 1–51, 2017. URL <http://arxiv.org/abs/1705.06206>.
- [6] A. Kitaev. *Fault-tolerant quantum computation by anyons*. pages 1–27, 1997. ISSN 00034916. doi: 10.1016/S0003-4916(02)00018-0. URL <http://arxiv.org/abs/quant-ph/9707021> [http://dx.doi.org/10.1016/S0003-4916\(02\)00018-0](http://dx.doi.org/10.1016/S0003-4916(02)00018-0).
- [7] P. Ferguson. *Topological Superconductors, Their Classification, and Majoranas: a Short Review*, 2018.
- [8] T. Stanescu. *Introduction to topological quantum matter and quantum computation*. 2017. ISBN 9781482245936.
- [9] C. W. J. Beenakker. *Search for Majorana fermions in superconductors*. (April 2012), 2011. ISSN 1947-5454. doi: 10.1146/annurev-conmatphys-030212-184337. URL <http://arxiv.org/abs/1112.1950> <http://dx.doi.org/10.1146/annurev-conmatphys-030212-184337>.
- [10] S. Sarma, M. Freedman, and C. Nayak. *Majorana Zero Modes and Topological Quantum Computation*. pages 1–16, 2015. ISSN 2056-6387. doi: 10.1038/npjqi.2015.1. URL <http://arxiv.org/abs/1501.02813> <http://dx.doi.org/10.1038/npjqi.2015.1>.
- [11] E. Majorana. Teoria simmetrica dell elettrone e del positrone. *Nuovo Cimento*, 5: 171–184, 1937.
- [12] F. Wilczek. *Lectures on Fractional Statistics and Anyon Superconductivity*. 1989.

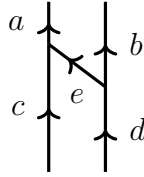
-
- [13] M. Freedman, M. Larsen, and Z. Wang. *A Modular Functor Which is Universal for Quantum Computation*. *Communications in Mathematical Physics*, 227(3): 605–622, Jun 2002. ISSN 1432-0916. doi: 10.1007/s002200200645. URL <https://doi.org/10.1007/s002200200645>.
 - [14] Z. Fan and H. De Garis. *Braid matrices and quantum gates for Ising anyons topological quantum computation*. *European Physical Journal B*, 74(3):419–427, 2010. ISSN 14346028. doi: 10.1140/epjb/e2010-00087-4.
 - [15] C. Nayak, S. Simon, A. Stern, M. Freedman, and S. Das Sarma. *Non-Abelian anyons and topological quantum computation*. *Reviews of Modern Physics*, 80(3):1083–1159, 2008. ISSN 00346861. doi: 10.1103/RevModPhys.80.1083.
 - [16] P. Bonderson, M. Freedman, and C. Nayak. *Measurement-Only Topological Quantum Computation*. 2008.
 - [17] A. Kitaev. *Unpaired majorana fermions in quantum wires*. *Physics-Uspekhi*, 44(10S): 131–136, October 2001. ISSN 1063-7869.
 - [18] S. Elliott and M. Franz. *Colloquium: Majorana fermions in nuclear, particle, and solid-state physics*. *Reviews of Modern Physics*, 87(1), 2015. ISSN 15390756. doi: 10.1103/RevModPhys.87.137.
 - [19] A. Bernevig and T. Neupert. *Topological Superconductors and Category Theory*. @BULLET 7th School on Mathematical Physics, pages 25–29, 2015.
 - [20] S. D. Sarma, M. Freedman, and C. Nayak. *Topological quantum computation*. *Physics Today*, 59(7):32–38, 2006. ISSN 0031-9228. doi: 10.1063/1.2337825. URL <http://physicstoday.scitation.org/doi/10.1063/1.2337825>.
 - [21] Z. Wang. *Topological Quantum Computation*. American Mathematical Society, 2010.
 - [22] J. Fuchs, I. Runkel, and C. Schweigert. *TFT construction of RCFT correlators I: partition functions*. *Nuclear Physics, Section B*, 646(3):353–497, 2002. ISSN 0550-3213.
 - [23] P.H. Bonderson and J.P. Preskill. *Non-Abelian Anyons and Interferometry*. CIT theses. California Institute of Technology, 2007. URL <https://books.google.co.uk/books?id=Wj04QwAACAAJ>.
 - [24] S. Eliëns. *Anyon Condensation: Topological Symmetry Breaking Phase Transitions and Commutative Algebra Objects in Braided Tensor Categories*, 2003.
 - [25] B. M. Ayeni. *Studies of Braided non-Abelian Anyons using Anyonic Tensor Networks*, 2017.
 - [26] A. Kitaev. *Anyons in an exactly solved model and beyond*. *Annals of Physics*, 321(1):2 – 111, 2006. ISSN 0003-4916. doi: <https://doi.org/10.1016/j.aop.2005.10.005>. URL <http://www.sciencedirect.com/science/article/pii/S0003491605002381>. January Special Issue.

-
- [27] A. Romito and Y. Gefen. *Ubiquitous Nonlocal Entanglement with Majorana Zero Modes*. *Physical Review Letters*, 119(15):1–5, 2017. ISSN 10797114. doi: 10.1103/PhysRevLett.119.157702.
 - [28] D. A. Ivanov. *Non-Abelian statistics of half-quantum vortices in p-wave superconductors*. *Physical Review Letters*, 86(2):268–271, 2001. ISSN 00319007. doi: 10.1103/PhysRevLett.86.268.
 - [29] J. Alicea, Y. Oreg, G. Refael, F. Von Oppen, and M. Fisher. *Non-Abelian statistics and topological quantum information processing in 1D wire networks*. *Nature Physics*, 7(5):412–417, 2011. ISSN 17452473. doi: 10.1038/nphys1915. URL <http://dx.doi.org/10.1038/nphys1915>.
 - [30] M. Leijnse and K. Flensberg. *Introduction to topological superconductivity and Majorana fermions*. *Semiconductor Science and Technology*, 27(12):1–21, 2012. ISSN 02681242. doi: 10.1088/0268-1242/27/12/124003.
 - [31] P. Bonderson. *Measurement-Only Topological Quantum Computation via Tunable Interactions*. 2013.
 - [32] J. Alicea. *New directions in the pursuit of Majorana fermions in solid state systems*. *Reports on Progress in Physics*, 75(7), 2012. ISSN 00344885. doi: 10.1088/0034-4885/75/7/076501.
 - [33] D. Aasen, M. Hell, R. Mishmash, A. Higginbotham, J. Danon, M. Leijnse, T. Jespersen, J. Folk, C. Marcus, K. Flensberg, and J. Alicea. *Milestones toward Majorana-based quantum computing*. *Physical Review X*, 6(3):1–28, 2016. ISSN 21603308. doi: 10.1103/PhysRevX.6.031016.
 - [34] S. Trebst, M. Troyer, Z. Wang, and A. Ludwig. *A short introduction to Fibonacci anyon models*. (1), 2009. ISSN 0375-9687. doi: 10.1143/PTPS.176.384. URL <http://arxiv.org/abs/0902.3275>{%}0A<http://dx.doi.org/10.1143/PTPS.176.384>.
 - [35] S. Vijay and L. Fu. *Teleportation-based quantum information processing with Majorana zero modes*. *Physical Review B*, 235446(23):1–9, 2016. ISSN 24699969. doi: 10.1103/PhysRevB.94.235446.

Appendix A

2-2 F-move Relation Derivation

Lets begin with the following diagram,



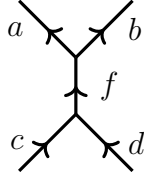
One can introduce the resolution of the identity (2.19),

$$\sum_f \sqrt{\frac{d_f}{d_c d_d}} \begin{array}{c} \begin{array}{c} a \nearrow \quad \nwarrow b \\ \quad \quad \quad e \\ \quad \quad \quad \nearrow \quad \nwarrow \\ c \quad \quad \quad d \\ \quad \quad \quad \nearrow \quad \nwarrow \\ \quad \quad \quad f \\ c \quad \quad \quad d \end{array} \end{array} = \sum_f \sqrt{\frac{d_f}{d_c d_d}} \begin{array}{c} \begin{array}{c} a \nearrow \quad \nwarrow b \\ \quad \quad \quad e \\ \quad \quad \quad \nearrow \quad \nwarrow \\ c \quad \quad \quad d \\ \quad \quad \quad \nearrow \quad \nwarrow \\ \quad \quad \quad f \\ c \quad \quad \quad d \end{array} \end{array}$$

Now using the definition of the F-move on the red section of the diagram,

$$= \sum_{f,g} \sqrt{\frac{d_f}{d_c d_d}} [(F_f^{ceb})^{-1}]_{dg} \begin{array}{c} \begin{array}{c} a \nearrow \quad \nwarrow b \\ \quad \quad \quad e \\ \quad \quad \quad \nearrow \quad \nwarrow \\ c \quad \quad \quad d \\ \quad \quad \quad \nearrow \quad \nwarrow \\ \quad \quad \quad f \\ c \quad \quad \quad d \end{array} \end{array} = \sum_{f,g} \sqrt{\frac{d_f}{d_c d_d}} [(F_f^{ceb})^{-1}]_{dg} \begin{array}{c} \begin{array}{c} a \nearrow \quad \nwarrow b \\ \quad \quad \quad e \\ \quad \quad \quad \nearrow \quad \nwarrow \\ c \quad \quad \quad d \\ \quad \quad \quad \nearrow \quad \nwarrow \\ \quad \quad \quad f \\ c \quad \quad \quad d \end{array} \end{array}$$

Finally using (2.16) for the blue section,

$$= \sum_f \sqrt{\frac{d_e d_f}{d_a d_d}} [(F_f^{ceb})^{-1}]_{da}$$


Therefore 2-2 F-move is related to the F-move as,

$$[F_{cd}^{ab}]_{ef} = \sqrt{\frac{d_e d_f}{d_a d_d}} [F_f^{ceb}]_{ad}^*,$$

where the following relation (which is a consequence of unitarity) was used,

$$[F_d^{abc}]_{fe}^\dagger = [F_d^{abc}]_{ef}^* = [F_d^{abc}]_{fe}^{-1}.$$

Diagrammatically the adjoint corresponds to reflecting in the horizontal plane so that the top and bottom of the diagram switch and the orientation of the arrows are reversed.

Appendix B

Pentagon Equation for Anyon Models

The Pentagon is most simply stated in terms of the following commutative diagram:

$$\begin{array}{ccccc}
 & & \oplus_{p,t} V_p^{xy} \otimes V_u^{pt} \otimes V_t^{zw} & & \\
 & \nearrow F_u^{pzw} & & \nwarrow F_u^{xyt} & \\
 \oplus_{p,q} V_p^{xy} \otimes V_q^{pz} \otimes V_u^{qw} & & & & \oplus_{s,t} V_u^{xs} \otimes V_s^{yt} \otimes V_t^{zw} \\
 & \searrow F_q^{xyz} & & \nearrow F_s^{yzw} & \\
 \oplus_{q,r} V_q^{xr} \otimes V_r^{yz} \otimes V_u^{qw} & \xrightarrow{F_u^{xrw}} & & \oplus_{r,s} V_u^{xs} \otimes V_r^{yz} \otimes V_s^{rw} &
 \end{array}$$

Here the sums in the F-moves have been dropped. The F-move are all tensored with the identity operation on the space they do not act in, for example, F_u^{pzw} means $\sum_u F_u^{pzw} \otimes \text{id}_{V_u^{qw}}$.

Appendix C

Calculation of Two-Sequence Phases

Consider (4.9) in the second form,

$$S_{12,24} = \begin{array}{c} \begin{array}{cccc} a_1 & & a_2 & a_3 & a_4 \\ & \nearrow & & \nearrow & \\ & \text{A}' & & \text{B}' & \\ & \downarrow & & \downarrow & \\ b_{12} & & b'_{23} & & b_{24} \\ & \nearrow & & \nearrow & \\ & \text{C} & & \text{D} & \\ & \downarrow & & \downarrow & \\ & \text{A} & & \text{B} & \\ a_1 & a_2 & a_3 & & a_4 \end{array} \\ = \begin{array}{cccc} a_1 & & a_2 & a_3 & a_4 \\ & \nearrow & & \nearrow & \\ & & b'_{23} & & \text{B}' \\ & & \downarrow & & \downarrow \\ & & a_3 & & \text{D} \\ & & \downarrow & & \downarrow \\ & & \bar{b}_{12} & & \bar{a}_2 \\ & & \downarrow & & \downarrow \\ & & \text{A} & & \text{B} \\ a_1 & a_2 & a_3 & & a_4 \end{array} \end{array} \quad (\text{C.1})$$

This follows simply from isotropy invariance, that is, one can move the A' vertex “along” the \bar{a}_2 charge line. If one looks at the red charge lines in the following equation, it is easy to see that they can be manipulated using an F-move,

$$\begin{array}{c} \begin{array}{cccc} a_1 & & a_2 & a_3 & a_4 \\ & \nearrow & & \nearrow & \\ & & b'_{23} & & \text{B}' \\ & & \downarrow & & \downarrow \\ & & a_3 & & \text{D} \\ & & \downarrow & & \downarrow \\ & & \bar{b}_{12} & & \bar{a}_2 \\ & & \downarrow & & \downarrow \\ & & \text{A} & & \text{B} \\ a_1 & a_2 & a_3 & & a_4 \end{array} \\ = \left[F_{a_4}^{b_{12}a_1b_{24}} \right]_{\bar{a}_2c} \begin{array}{cccc} a_1 & & a_2 & a_3 & a_4 \\ & \nearrow & & \nearrow & \\ & & b'_{23} & & \text{B}' \\ & & \downarrow & & \downarrow \\ & & a_3 & & \text{D} \\ & & \downarrow & & \downarrow \\ & & \bar{b}_{12} & & c \\ & & \downarrow & & \downarrow \\ & & \text{A} & & \text{B} \\ a_1 & a_2 & a_3 & & a_4 \end{array} \end{array}, \quad (\text{C.2})$$

where $c = \bar{a}_1 \times a_2 \times a_4$. Repeating this process,

$$= \left[F_{a_3}^{b'_{23} a_4 \bar{b}_{24}} \right]_{\bar{a}_2 d} , \quad (\text{C.3})$$

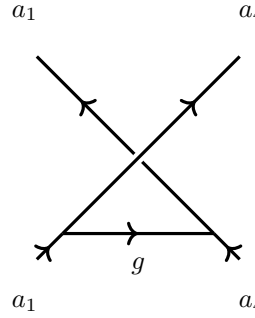
where $d = a_2 \times a_3 \times a_4$. The last F-move allowed the \mathbf{B}' vertex to move past the \mathbf{D} vertex. This process is now again repeated to move the \mathbf{B}' vertex past the \mathbf{C} vertex. Now the bottom half of the diagrams are becoming quite crowded, so one can use (4.11)—before it was used in Sec.4.2—to dissociate the b_{23} and b'_{23} from the \mathbf{C} vertex and \mathbf{D} vertex respectively, to clarify the diagram.

$$= \left[F_{b_{24}}^{a_2 b_{23} d} \right]_{a_3 a_4} \otimes \Pi_{23}^{(b_{23})} \quad (\text{C.4})$$

where the F-move associated with the dissociation is not included here. Isolating the “rectangular” part of the diagram,

$$\begin{array}{c}
 \begin{array}{ccc}
 a_1 & & a_4 \\
 & \nearrow \bar{b}_{24} & \searrow \\
 \text{B} & & \text{B}' \\
 \bar{a}_2 & & c \\
 \text{A} & & \text{A}' \\
 & \nwarrow \bar{b}_{12} & \nearrow \\
 a_1 & & a_4
 \end{array}
 = [F_{a_1}^{a_1 \bar{b}_{24} b_{12}}]_{a_3 \tilde{g}} [F_{a_4}^{b_{12} b_{24} a_4}]_{a_2 g}
 \begin{array}{ccc}
 a_1 & & a_4 \\
 & \nearrow \tilde{g} & \searrow \\
 \text{A} & & \text{A}' \\
 & \text{B} & \text{B}' \\
 & \nwarrow b_{12} & \nearrow \\
 a_1 & & a_4
 \end{array}
 \end{array} \quad (\text{C.5})$$

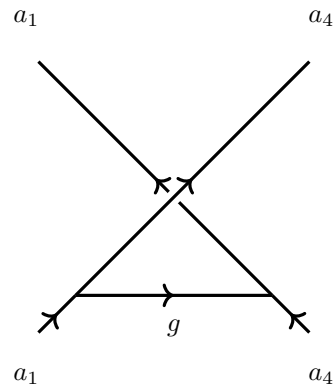
where $g, \tilde{g} = b_{12} \times \bar{b}_{24}$. Then using the (2.16) it is clear that $g = \tilde{g}$ and the sequence $S_{12,24} = \hat{X}_{14} \otimes \Pi_{23}^{(b_{23})}$ is finally,

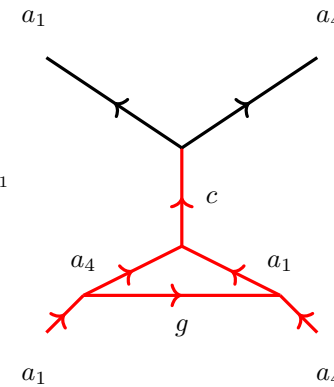
$$\hat{X}_{14} = [F_{a_3}^{b'_{23} a_4 \bar{b}_{24}}]_{\bar{a}_2 d} [F_{b_{24}}^{a_2 b_{23} d}]_{a_3 a_4} [F_{a_1}^{a_1 \bar{b}_{24} b_{12}}]_{a_3 \tilde{g}} [F_{a_4}^{b_{12} b_{24} a_4}]_{a_2 g}$$


$$\quad (\text{C.6})$$

Using the Ising anyon model in Table.4.1 one can see that none of these vanish since they all obey the fusion rules and also that they are all phases. Therefore dropping them in the thesis was justified.

Now to show that this is the braiding operator in (4.14) one uses (2.28),

$$\hat{X}_{14} =$$


$$= \sum_c R_c^{a_4 a_1}$$


$$\quad (\text{C.7})$$

$$\hat{X}_{14} = \sum_c [F_c^{a_4 g a_4}]_{a_1 a_1} R_c^{a_4 a_1} \quad (C.8)$$

Using (2.16) it is clear that the loop reduces to a line, therefore,

$$\hat{X}_{14} = \sum_c [F_c^{a_4 g a_4}]_{a_1 a_1} R_c^{a_4 a_1} \text{ (diagram of a vertex with two incoming lines and one outgoing line)} = \sum_c [F_c^{a_4 g a_4}]_{a_1 a_1} R_c^{a_4 a_1} \Pi_{14}^{(c)}. \quad (\text{C.9})$$

Let's return to the previous diagrams and show that the above diagram can indeed be dissociated. The reason this was omitted before is that “rectangular” part of diagram along with the projection part causes the diagram to look cluttered. So now that it has been shown that the “rectangle” can be reduced to line, the diagram is clearer and one can use the 2-2 F-move in (2.22) to show,

$$= \sum_h \left[F_{a_4 b_{23}}^{b'_{23} a_4} \right]^{-1} \quad (C.10)$$

Now using the relation in (2.23), $[F_{a_4 b_{23}}^{b'_{23} a_4}]^{-1} = [F_{a_5}^{a_4 h a_4}]_{b_{23} b'_{23}}$, which is allowed by the Ising anyon fusion rules and is not in Table.4.1, and is trivial.

Appendix D

List of the Remaining Three-Sequences

